Available online at www.sciencedirect.com
SCIENCE DIRECT®
Nuclear Physics A 766 (2006) 25–51
NUCLEAR PHYSICS A

Experimental and theoretical investigations of quadrupole collective degrees of freedom in ^{104}Ru

J. Srebrny [a,*,1], T. Czosnyka [b], Ch. Droste [a], S.G. Rohoziński [a], L. Próchniak [c], K. Zając [c], K. Pomorski [c], D. Cline [d], C.Y. Wu [d], A. Bäcklin [e], L. Hasselgren [e], R.M. Diamond [f], D. Habs [g], H.J. Körner [h,✠], F.S. Stephens [f], C. Baktash [i], R.P. Kostecki [a]

[a] *Faculty of Physics, Warsaw University, Warsaw 00-681, Poland*
[b] *Heavy Ion Laboratory, Warsaw University, Warsaw 02-093, Poland*
[c] *Institute of Physics, The Maria Curie-Skłodowska University, 20-031 Lublin, Poland*
[d] *Nuclear Structure Research Laboratory, University of Rochester, Rochester, NY 14627, USA*
[e] *Department of Radiation Sciences and The Svedberg Laboratory, Uppsala University, S-75121, Sweden*
[f] *Lawrence Berkeley Laboratory, Berkeley, CA 94720, USA*
[g] *Ludvig-Maximilian University, Münich, D-8046 Garching, Germany*
[h] *Technical University, Münich, D-8046 Garching, Germany*
[i] *HRIBF, P.O. Box 2008, Oak Ridge, TN 37831, USA*

Received 1 August 2005; received in revised form 15 November 2005; accepted 15 November 2005

Available online 6 December 2005

Abstract

The magnitudes and signs of twenty eight E2 and three M1 matrix elements involving 17 low-lying excited states in ^{104}Ru have been measured by Coulomb excitation using ^{208}Pb, ^{136}Xe and ^{58}Ni ions. The completeness of the set of E2 matrix elements is sufficient to extract, directly from the data, the expectation values of the intrinsic-frame E2 moments that provide considerable insight into the underlying collectivity. The measured E2 properties strongly correlate with macroscopic quadrupole collective degrees of freedom. Detailed comparison of the experimental results and theoretical microscopic calculations within the general quadrupole collective Bohr Hamiltonian are presented. Very good agreement of calculations and experiment is achieved without any parameters fitted to the ^{104}Ru experimental data. Results of phenomenological γ-unstable and γ-rigid models are also given.

* Corresponding author.
E-mail address: js@npdaxp.fuw.edu.pl (J. Srebrny).
[1] Present address: Heavy Ion Laboratory, Warsaw University, Warsaw 02-093, Poland.
✠ Deceased.

0375-9474/$ – see front matter
doi:10.1016/j.nuclphysa.2005.11.013

PACS: 21.60.Ev; 23.20.Js; 23.20.Lv; 25.70.De

Keywords: NUCLEAR REACTIONS ^{104}Ru(^{208}Pb, ^{208}Pb′), $E = 954$ MeV; ^{104}Ru(^{136}Xe, ^{136}Xe′), $E = 525$ MeV; ^{104}Ru(^{58}Ni, ^{58}Ni′), $E = 165$ MeV, 190 MeV; measured E_γ, I_γ, (particle) γ-coin following Coulomb excitation. ^{104}Ru deduced levels, J, π, E2 and M1 matrix elements, quadrupole collectivity. Comparison with model predictions.

1. Introduction

The present paper reports on the use of heavy-ion induced Coulomb excitation to measure a set of twenty eight E2 and three M1 matrix elements involving the lowest-lying states in ^{104}Ru. The goal of this work is to test the validity of collective model descriptions of the structure of ^{104}Ru and to evaluate the available collective model calculations.

An important step in the field of heavy ion induced Coulomb excitation was achieved due to the development of beams of the heaviest ions combined with position sensitive detection systems for the scattered projectiles and recoiling target nuclei. This makes it possible to Coulomb excite states up to high spin and to measure both the signs and magnitudes of the practically complete set of E2 matrix elements for the low-lying states in a nucleus [1]. Extraction of these E2 matrix elements is far from trivial for heavy ion induced Coulomb excitation because the strong coupling leads to a complicated dependence of the data on the matrix elements. Sets of data from the Coulomb excitation experiments having a wide range of projectile Z values and scattering angles made it possible to obtain a model independent set of E2 transition matrix elements.

Heavy ion induced Coulomb excitation of ^{104}Ru nucleus was studied by Stachel et al. by using ^{208}Pb projectiles and ^{104}Ru target [2] as well as by using inverse kinematics bombarding a ^{208}Pb target with a ^{104}Ru beam [3]. The analysis of the data were performed using a least-square code specially developed in GSI (see [3] for details). Here, we present results of heavy ion induced Coulomb excitation of ^{104}Ru target using ^{58}Ni, ^{136}Xe and ^{208}Pb projectiles. Our data have been analysed using the Rochester–Warsaw coupled-channel Coulomb excitation least-square search code GOSIA [4]. The final results of these two independent sets of experiments are in very good agreement. In our case, the use of three projectile species enable measurement of the diagonal E2 matrix elements for the 2_2^+ band and to identify the 0_2^+ band.

The set of E2 matrix elements measured in the present work is sufficiently complete to allow, for the low-lying states, the expectation values of the E2 moments in the intrinsic frame to be deduced directly from the data. It should be noted that these model-independent intrinsic-frame E2 moments are directly related to the collective behaviour of the nucleus. They provide a direct measure of the extent to which the properties of the low-lying states in ^{104}Ru can be correlated using only quadrupole collective degrees of freedom. Application of the non-energy-weighted sum rules technique [1,5,6] as a model-independent analysis of the Coulomb excitation data is used to determine unambiguously the underlying collective correlations for the low-lying levels in ^{104}Ru.

The knowledge of a nearly complete set of E2 matrix elements for low-lying levels in case of a shape transitional nucleus like ^{104}Ru provides a formidable challenge to nuclear structure theory. The data concerning ^{104}Ru obtained in GSI [2,3] have been successfully confronted with the IBM model [7–9]. However the IBM quadrupole operator is not appropriate for applying the sum rule technique [10]. The entire data are confronted to calculations performed in the frame of a geometrical collective model. This Hamiltonian is obtained from a more general "quadrupole plus pairing" collective model through the Born–Oppenheimer approximation which takes into account the effect of coupling with the pairing vibrations [11]. All inertial functions and the

potential were determined from a microscopic theory. Without any parameters fitted to ^{104}Ru experimental data, we obtain good agreement between the experimental and theoretical results.

Exact formulae for the collective quadrupole invariants as functions of the Bohr parameters, β and γ, of the ellipsoidal deformation are derived in Appendix A.

2. The experimental method

All the experiments used the same selfsupporting ruthenium target 0.69 mg/cm^2 thick, enriched to 99.3% in ^{104}Ru. The target was produced using an Ar beam to sputter enriched Ru powder onto an Al foil, naturally covered by a Al_2O_3 film. The Al_2O_3 crystal structure is very similar to that of ruthenium and create a good starting point for Ru foil crystal growth. After the sputtering procedure, the Al foil was dissolved by a special solution neutral to ruthenium producing a self supporting foil.

2.1. Coulomb excitation using ^{208}Pb ions

A 954 MeV ^{208}Pb beam from the SuperHILAC at the Lawrence Berkeley Laboratory was used to Coulomb excite the ^{104}Ru target. The recoiling target nuclei were detected at ^{208}Pb scattering angles between $160^\circ < \Theta_{\rm cm} < 180^\circ$ by a circular Si detector placed at 0° to the beam direction and covered by a ^{208}Pb foil of thickness sufficient to stop the incident ^{208}Pb. The de-excitation gamma rays were detected by three Ge detectors, at angles of 0°, $+100^\circ$ and -100° to the incident beam, in coincidence with the recoiling ^{104}Ru target nuclei detected in the Si detector. In addition, four 7.6 cm diameter by 7.6 cm long NaI detectors were placed around the target to serve as a multiplicity filter to identify the gamma-ray decay scheme. The large recoil velocity, 12.5% of the velocity of light, produced large Doppler broadening of the detected gamma rays due to the finite size of the gamma-ray detectors. In the final analysis, only the Coulomb excitation yields for the Ge detector at $\Theta = 0^\circ$ were used since this detector had the smallest Doppler broadening effect. Fig. 1 shows spectrum of gamma-rays being in coincidence with Ru recoils. The achieved energy resolution was 0.75% at 500 keV. Fig. 2 presents the level scheme of ^{104}Ru excited in the experiment, showing all observed transitions.

The ^{208}Pb experiment was performed using an incident energy of 4.6 MeV A which exceeds the safe energy criterion [12] required to ensure that the interaction is purely electromagnetic, that is, for heavy ions the distance of closest approach should exceed $1.25(A_p^{1/3} + A_t^{1/3}) + 5$ fm to ensure less than 0.1% deviation from Coulomb scattering theory. This criterion corresponds to a bombarding energy of 4.1 MeV A. The higher bombarding energy was used to optimize the population of high-spin states. The experimental Coulomb excitation yields were corrected by up to 10% to account for the influence of Coulomb-nuclear interference effects and the errors were increased to exceed the size of the correction used. This correction was estimated using a study of this effect by Guidry et al. [13]. The assigned errors were enlarged further to reflect the ± 10 MeV uncertainty in the bombarding energy and the 3% uncertainty in the Ge detector efficiency which was measured using calibrated gamma-ray sources.

2.2. Coulomb excitations using ^{136}Xe ions

A 525 MeV ^{136}Xe beam from the SuperHILAC at the Lawrence Berkeley Laboratory was used. Recoiling target nuclei as well as scattered ^{136}Xe ions were detected by two position sensitive rectangular PPAC covering $\Theta_{\rm lab}$ angle 17.5°–38.5°, and 39°–63°. The de-excitation

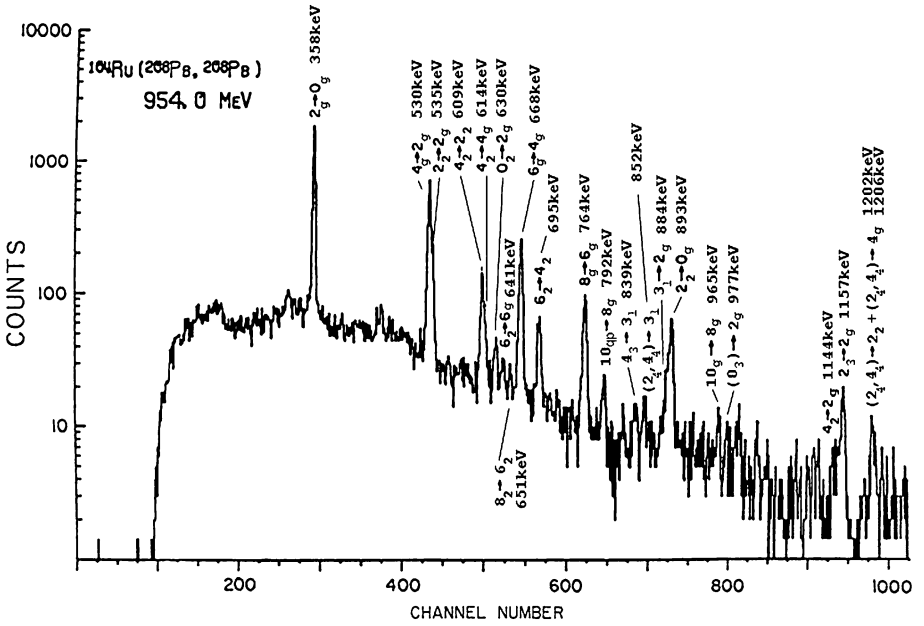

Fig. 1. Doppler corrected gamma-ray spectrum registered in 0° Ge detector in coincidence with recoiled ^{104}Ru target nuclei registered in 0° Si detector.

gamma rays were detected by two Ge detectors placed at angles of 127.5° and 152.5° to incident beam, in coincidence with the recoiling Ru target nuclei and scattered Xe beam nuclei. After an event by event Doppler correction 1% gamma-ray energy resolution was achieved. In the final Coulomb excitation analysis the γ-yields were integrated over three regions of Xe scattering angles $\Theta_{\mathrm{cm}} \in \{54°–90°, 102°–116°, 116°–130°\}$.

2.3. Coulomb excitation using ^{58}Ni ions

Two separate experiments were performed. One experiment used a 165.5 MeV ^{58}Ni beam from the Tandem Van de Graaff accelerator at the University of Rochester. Scattered ^{58}Ni ions were detected by circular Si detectors in coincidence with de-excitation gamma rays detected by Ge gamma-ray detectors at 1.5° and 60° to the beam. The particle detectors were placed at laboratory scattering angles of 119°, 105°, 76.0°, 61.5°, 47.5° as well as an annular Si detector covering the angular range from 163° to 175°. The angles of the particle detectors were determined with accuracy up to 0.5° using the measured elastic scattering data.

The second experiment employed a 190 MeV ^{58}Ni beam from the Tandem Van de Graaff accelerator at the Brookhaven National Laboratory. The scattered ^{58}Ni ions were detected by an annular Si detector, subtending the angular range from 155° to 175°, in coincidence with de-excitation gamma rays observed by Ge detectors at 0° and 110°. In contrast to the other ^{58}Ni experiment, this experiment used an incident energy 11 MeV above the Cline safe energy criterion [12]. However, no effect due to Coulomb-nuclear interference was manifest within the experimental errors.

For the 165.5 MeV ^{58}Ni beam experiment the energy resolution of the Si detectors was sufficient to resolve the scattered ^{58}Ni and recoiling ^{104}Ru target nuclei in the forward detectors

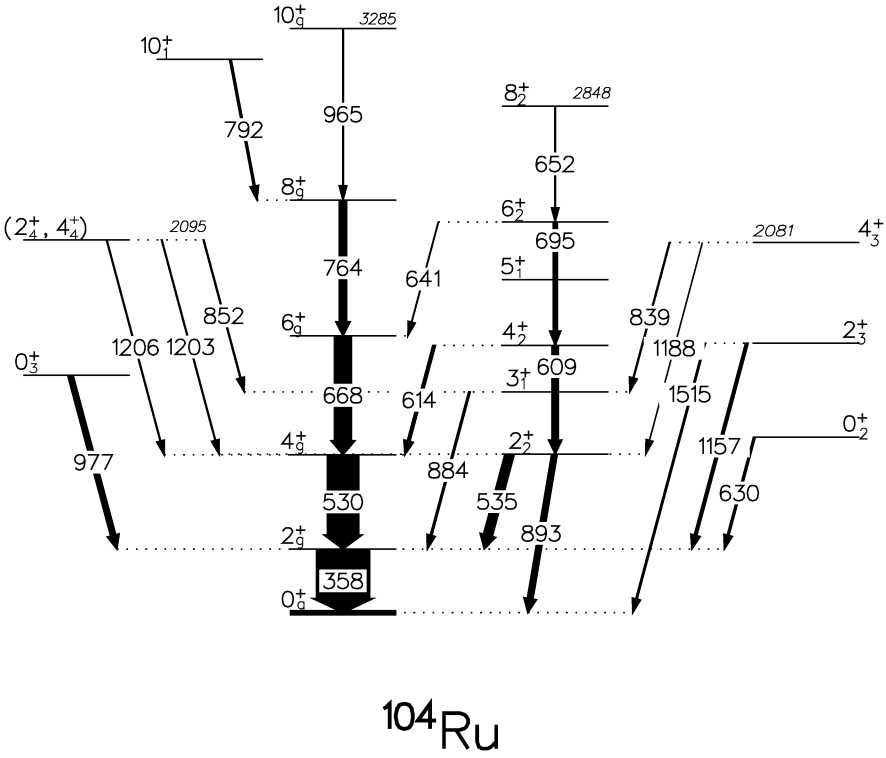

Fig. 2. Partial ^{104}Ru level scheme showing all levels observed in present paper. Arrow widths are proportional to γ-ray intensities observed in ^{208}Pb experiment.

and to allow Doppler correction for different slices of energy loss in the target. The gamma-ray spectrum from the 190 MeV experiment is shown in Fig. 3. An energy resolution of 0.5% for 500 keV was achieved.

3. Level scheme for ^{104}Ru

The level scheme of ^{104}Ru, shown in Fig. 2, is based on prior work [3,14] and [15] which is confirmed by the present work. For the present ^{208}Pb beam experiment the ground band was seen up to the 10^+_g level and $10^+_{\rm qp}$, the 2^+_2 band up to 8^+_2, the 0^+_2 band up to 4^+_3, only one 0^+ level from the 0^+_3 band, and one additional level 2095 keV energy of spin and parity valued 2^+_4 or 4^+_4. For the ^{136}Xe beam, the ground band was excited up to 8^+_g level, the 2^+_2 band up to 6^+_2 level with the 8^+_2 level weekly excited, and the 0^+_2 band up to 4^+_3 level was excited. For the ^{58}Ni beam the ground band was observed up to 8^+_g level, the 2^+_2 band up to 6^+_2 level, the 0^+_2 band up to 4^+_3 level, and additionally the $(2^+_4, 4^+_4)$ level 2095 keV energy.

For the 2081 keV level spin and parity 4^+_3 were assigned based on relative intensities of four γ-transitions depopulating the level to 2^+_g, 2^+_2, 3^+_1 and 2^+_3 (see [14] and reference given therein). Large matrix elements $\langle 4_3 \| \mathrm{E2} \| 2_3 \rangle = 0.75(25)$ eb and $\langle 2_3 \| \mathrm{E2} \| 0_2 \rangle = 0.71(4)$ eb confirm the assignment of the 4^+_3 and 2^+_3 levels to the 0^+_2 band.

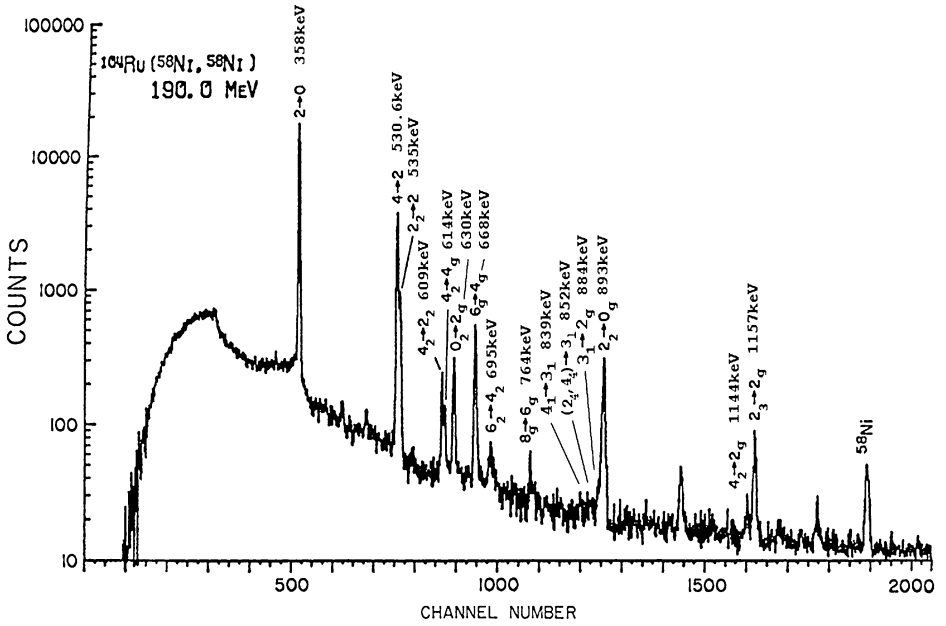

Fig. 3. Doppler corrected gamma-ray spectrum registered in 0° Ge detector in coincidence with backscattered ^{58}Ni beam nuclei.

4. Extraction of E2 matrix elements from the Coulomb excitation data

Extraction of the E2 matrix elements from heavy-ion induced Coulomb excitation data is an extremely difficult task because of the dramatic increase in the number of unknown matrix elements involved when many states are excited. For example, in the present case the Coulomb excitation cross sections depend in a complicated non-linear way on the signs and magnitudes of the 96 matrix elements coupling the 26 states included in the analysis.

In the present work, de-excitation gamma-ray transitions were observed involving 17 states. However, virtual excitation of other states can influence the excitation of the observed states. Consequently, the present analysis assumed additional states extending the observed bands. The energy (spin) of these states were assumed to be as follows: for the 2 qp band at 3.96 MeV (12^+) and for the ground band 4.4 MeV (12^+); for the 2_2^+ band at 1.872 and 2.9 MeV (5^+), 3.13 MeV (8^+) and 4.0 MeV (10^+); for the 0_2^+ band at 2.75 MeV (6^+); for the 0_3^+ band at 1.75 MeV (2^+). The energies and matrix elements involving these additional states were taken to be a smooth extrapolation of the measured values. Note that 60 matrix elements, including those involving the additional states assumed in the present analysis, were insensitive to the data set and thus were not determined. Conversely, the final results are insensitive to the properties assumed for these additional states.

The semiclassical Coulomb excitation, coupled-channel, least-squares search code GOSIA [4] was developed as a practical approach for the analysis of heavy-ion Coulomb excitation experiments and this code was used for the final analysis of the present data. The 50-level coupled-channel code GOSIA can make a least-squares fit up to 300 matrix elements (E1, E2, E3, E4, E5, E6, M1, M2) to several thousand data from up to 50 independent Coulomb excitation experiments, as well as other lifetime, static moment, branching ratio and E2/M1 mixing

ratio data. Pseudo-analytical approximations are used to calculate the derivatives needed for the deepest-descent minimalization, resulting in several orders of magnitude increase in speed compared to a full calculation. The code allows integration over target thickness and the finite size of the detectors and includes the recoil motion transformation to second order in recoil velocity.

In general, model independence of extracted matrix elements can be achieved using sets of random numbers as initial values for the unknown matrix elements in the least-squares search in order to eliminate bias. However, the procedure used in the present analysis was to start with the lightest ion data, which involves the fewest states, and then progressively add heavier ion data, at each stage varying the signs and magnitudes of the matrix elements by hand in order to test the results for uniqueness and to eliminate the influence of a possible bias. The many combinations of signs and magnitudes sampled suggest that the final solution is a unique one with the exception of some sign ambiguities to be mentioned later.

The errors of the fitted matrix elements are difficult to estimate because of the dominance of the cross-correlation effects for this strongly-coupled nonlinear system. Frequently used methods for error estimation are invalid for the present problem. For example the commonly used curvature matrix method is ill suited because of the limited validity of the second-order expansion and the unavoidable presence of nuisance parameters, i.e. parameters insensitive to the data, which must be filtered out prior to matrix inversion to prevent an ill-defined situation. Error estimation based on the assumption that the least-square statistic should obey the χ^2 distribution with a given number of degrees of freedom cannot be defined because of the wide range of sensitivity of the various parameters to the data. For the present analysis, worst-case errors were estimated for each parameter by perturbing the matrix element for which the error was being estimated and then executing a one-step minimisation on the remaining parameters in order to determine the maximum correlation path. The probability distribution then was constructed along that 68.3% of the total integrated probability lie between the error limits. Note that the positive and negative error values were calculated separately since the errors can be strongly asymmetric around the best value.

5. Various corrections and sources of systematic errors

The angular distribution of the de-excitation gamma rays from the excited nuclei recoiling in vacuum is perturbed due to the interaction of the static moments of the excited nuclear states with the highly ionized atomic configurations. This deorientation effect is taken into account using the two-state model of Brenn and Spehl [16] with the parameters derived from earlier Coulomb excitation measurements [18] on ^{186,188,190,192}Os and ^{194}Pt (for details see also [17]). It was found that a 20% change in the magnitude of this effect produced less than a 2% change in matrix elements extracted.

Virtual excitation of high-lying states can influence the excitation of low-lying states. Dipole polarization results from the influence on the excitation of low-lying collective states due to virtual excitation of the giant dipole resonance. Virtual excitations of the giant dipole resonance was taken into account using the concept of a polarization charge [19]. The effect is dependent on the center-of-mass bombarding energy and is expected to affect mostly high-lying levels excited in the Pb experiment. Switching off the correction or doubling its strength changes the excitation of the 10^+_g state by about 10%. This is within the experimental errors, as is true for all other excited states. M1 excitation has a negligible influence on the Coulomb excitation but features prominently in both the branching ratios and angular distributions for the gamma-ray de-excitation. Thus in the present work it was possible to determine 3 M1 transition matrix elements with

reasonable errors. The influence of E4 excitation was calculated to be negligible for Coulomb excitation using ^{58}Ni, ^{136}Xe and ^{208}Pb projectiles. It is of importance only when lighter ions are used. Including the known 3^- state in the calculations produced a 4% decrease in the $4_g^+ \to 2_g^+$ yield in the Pb experiment while all other yields were affected by less than 1%, that is, less than the statistical errors. This is in agreement with the findings of Wu [18].

Corrections due to atomic screening, vacuum polarization and relativistic effects were estimated [18] to be negligible. The semiclassical approximation used in the analysis is estimated to give the largest correction, that is, $< 5\%$ for ^{208}Pb and $< 10\%$ for ^{58}Ni. These sources of systematic error are comparable with the corrections due to Coulomb-nuclear interference. In the present calculations, no correction has been made for the use of the semiclassical approximation other than the use of symmetrized orbits [19].

6. Signs of matrix elements

The relative signs of the matrix elements involved have a significant influence on Coulomb excitation. This can be understood as due to interference between single-step amplitudes, involving a single matrix element, and multi-step amplitudes involving two or more matrix elements.

Tables 1 and 2 present signs and magnitudes of matrix elements as deduced from the present analysis. Note that signs of 28 matrix elements have been determined. The signs of the wave functions have been chosen in such a way that E2 reduced matrix elements (ME) for streched

Table 1
Diagonal E2 reduced matrix elements in eb units

State	Experiment (eb)		Theory[a]					
					Symmetry limit models			
			QCBH, pairing		DF γ-rigid, $\beta_0 = 0.28$		W–J γ-soft	
	Present	GSI [3]	std.	dyn.	$\gamma_0 = 25°$	$\gamma_0 = 30°$	$\beta_0 = 0.28$	$\beta_0 = 0$[b]
2_g^+	$-0.71(11)$	$-0.91(40)$	-0.77	-0.88	-0.80	-0.09	-0.12	-0.11
4_g^+	$-0.79(15)$	$-0.42(31)$	-1.10	-1.14	-0.63	-0.20	-0.20	-0.25
6_g^+	$-0.70(^{+30}_{-20})$	$-0.54(22)$	-1.41	-1.40	-0.68	-0.27	-0.29	-0.37
8_g^+	$-0.6(^{+3}_{-5})$	$-0.76(31)$	-1.71	-1.67	-0.76	-0.32	-0.38	-0.54
10_g^+	–		-2.04	-2.0	-0.83	-0.38	-0.47	-0.72
2_2^+	0.62(8)	–	0.59	0.73	0.80	0.11	0.04	0.05
3_1^+	–	–	0.0	0.0	0.0	0.0	0.0	0.0
4_2^+	$-0.58(18)$	–	-0.16	-0.32	-1.2	0.06	-0.07	-0.09
5_1^+	–	–	-0.70	-0.70	-0.68	-0.10	-0.12	-0.18
6_2^+	$\pm 1.0(3)$	–	-0.70	-0.87	-1.43	-0.02	-0.17	-0.24
8_2^+	–	–	-1.22	-1.29	-1.14	-0.10	-0.26	-0.40
2_3^+	$-0.08(^{+11}_{-25})$	–	-0.13	-0.72	–	–	-0.12	-0.18
4_3^+	–	–	0.49	0.32	–	–	-0.20	-0.33
6_3^+	–	–	0.15	-1.24	–	–	-0.17	-0.50
2_4^+	–	–	–	–	–	–	-0.06	-0.08
4_4^+	–	–	–	–	–	–	-0.07	0.10
4_5^+	–	–	–	–	–	–	-0.10	-0.16

[a] The theoretical model descriptions are given in Section 9.
[b] Harmonic vibrator.

Table 2
Transitional E2 reduced matrix elements

Transition	Experiment			Theory[a] Matrix element					
	Matrix element		Trans. prob.			Symmetry limit models			
	present	GSI [3]	present	QCBH, pairing		DF γ-rigid, $\beta = 0.28$		W–J γ-soft	
				std.	dyn.	$\gamma_0 = 25°$	$\gamma_0 = 30°$	$\beta_0 = 0.28$	$\beta_0 = 0$[b]
	$\langle f \Vert \mathrm{E2} \Vert i \rangle$ eb		B(E2) e^{2}b^2	$\langle f \Vert \mathrm{E2} \Vert i \rangle$ eb					
$2_g^+ \to 0_g^+$	0.917(25)	0.910	0.168(9)	0.838	0.816	0.955	0.936	0.919	0.799
$4_g^+ \to 2_g^+$	1.43(4)	1.47(8)	0.226(11)	1.45	1.38	1.51	1.48	1.55	1.52
$6_g^+ \to 4_g^+$	2.04(8)	2.09(9)	$0.320(^{+10}_{-26})$	1.97	1.84	2.02	1.99	2.10	2.23
$8_g^+ \to 6_g^+$	$2.59(^{+24}_{-9})$	2.49(8)	$0.39(^{+8}_{-3})$	2.44	2.26	2.43	2.39	2.61	2.95
$10_g^+ \to 8_g^+$	2.7(6)	2.64(27)	0.26(10)	2.88	2.66	2.78	2.73	3.09	3.66
$3_1^+ \to 2_2^+$	–	−1.22(10)		−1.19	−1.16	−1.52	−1.48	−1.30	−1.39
$4_2^+ \to 2_2^+$	1.12(5)	0.90(11)	0.139(11)	1.02	0.92	0.90	0.96	1.26	1.34
$4_2^+ \to 3_1^+$	–	±0.68(5)		−0.83	−0.95	−0.97	0	−0.12	−0.16
$5_1^+ \to 3_1^+$	–	1.2(4)		1.35	1.25	1.39	1.34	1.52	1.72
$6_2^+ \to 4_2^+$	1.52(12)	1.62(12)	$0.178(^{+30}_{-14})$	1.61	1.53	1.47	1.29	1.89	2.13
$8_2^+ \to 6_2^+$	2.0(4)	2.0(5)	$0.23(^{+6}_{-9})$	2.15	2.05	1.81	1.77	2.43	2.89
$2_3^+ \to 0_2^+$	0.71(4)	0.74(5)	0.101(13)	0.75	0.77	–	–	0.83	0.94
$4_3^+ \to 2_3^+$	0.75(25)	–	0.063(21)	0.47	0.67	–	–	1.46	1.70
$6_3^+ \to 4_3^+$				1.27	1.25	–	–	2.02	2.45
$2_4^+ \to 0_3^+$					−0.32	–	–	0.85	0.97
$4_4^+ \to 2_4^+$						–	–		
$6_4^+ \to 4_4^+$						–	–		
$2_2^+ \to 0_g^+$	−0.156(2)	−0.170(13)	0.0049(3)	0.022	−0.047	−0.108	0.09	0.097	0.082
$2_2^+ \to 2_g^+$	−0.75(4)	−0.85(7)	0.113(11)	−0.75	−0.52	−0.82	−1.12	−1.15	−1.13
$2_2^+ \to 4_g^+$	$\in [-0.1, 0.1]$	–		0.16	0.06	−0.25	0	0.08	0.09
$3_1^+ \to 2_g^+$	–	0.224(10)		0.01	−0.105	−0.17	−0.15	0.137	0.14
$3_1^+ \to 4_g^+$	–	−0.57( )		−0.54	−0.43	−1.00	1.1	−0.82	−0.88
$4_2^+ \to 2_g^+$	−0.107(8)	±0.072(9)	0.0013(2)	0.08	0.055	0.28	0	0.134	0.138
$4_2^+ \to 4_g^+$	−0.83(5)	−0.71(8)	0.0759(9)	−0.73	−0.57	−0.66	0.66	−1.21	−1.28
$5_1^+ \to 4_g^+$	–	–		0.04	−0.05	0.13	−0.18	0.18	0.21
$5_1^+ \to 6_g^+$	–	–		−0.63	−0.54	−1.11	1.17	−1.02	−1.15
$6_2^+ \to 4_g^+$	$-0.22(^{+6}_{-12})$	−0.080(10)		0.09	0.07	0.16	−0.09	0.16	0.19
$6_2^+ \to 6_g^+$	–	> -0.84		−0.75	−0.62	−0.52	0.57	−1.29	−1.45
$8_2^+ \to 6_g^+$	–	–		0.08	0.044	−0.09	−0.08	0.19	0.25
$8_2^+ \to 8_g^+$				−0.78	−0.67	−0.48	0.51	−1.36	−1.61
$0_2^+ \to 2_g^+$	−0.266(8)	−0.261(10)	0.071(4)	−0.31	−0.264	–	–	−0.292	−0.50
$0_2^+ \to 2_2^+$	0.08(3)	–	$0.007(^{+6}_{-4})$	−0.40	−0.30	–	–	−0.06	−0.10
$2_3^+ \to 0_g^+$	−0.071(10)	−0.07(5)	0.0010(3)	−0.041	−0.081	–	–	−0.036	0.008
$2_3^+ \to 2_g^+$	±0.07(3)	−0.11(5)	$0.0011(^{+12}_{-6})$	0.06	0.10	–	–	0.04	0.06
$2_3^+ \to 4_g^+$	−0.37(4)	−0.35(22)	0.028(6)	−0.41	−0.41	–	–	−0.47	−0.80
$2_3^+ \to 2_2^+$	$\pm 0.22(^{+25}_{-5})$	±0.23(23)	0.010(4)	0.35	0.32	–	–	0.35	0.59
$2_3^+ \to 4_2^+$	$0.31(^{+13}_{-6})$	–	$0.019(^{+25}_{-7})$	−0.35	−0.38	–	–	−0.08	−0.16
$2_3^+ \to 4_4^+$	$0.53(^{+32}_{-14})$	–		1.25	1.19	–	–	0.0004	0.0004
$0_3^+ \to 2_g^+$	> -0.1	–	< 0.017	−0.17	−0.08	–	–	−0.06	−0.06
$0_3^+ \to 2_2^+$	–	–		−0.11	−0.14	–	–	−0.58	−0.62
$0_3^+ \to 2_3^+$	–	–		−0.03	0.03	–	–	0.03	0.07

(*continued on next page*)

Table 2 (*continued*)

Transition	Experiment			Theory[a] Matrix element					
	Matrix element		Trans. prob.			Symmetry limit models			
	present	GSI [3]	present	QCBH, pairing		DF γ-rigid, $\beta = 0.28$		W–J γ-soft	
				std.	dyn.	$\gamma_0 = 25°$	$\gamma_0 = 30°$	$\beta_0 = 0.28$	$\beta_0 = 0$[b]
	$\langle f \Vert E2 \Vert i \rangle$ eb		B(E2) e^{2}b^2	$\langle f \Vert E2 \Vert i \rangle$ eb					
$2_3^+ \to 3_1^+$				0.76	0.51	–	–	0.08	0.0002
$2_4^+ \to 3_1^+$					0.49	–	–	0.96	1.08
$4_3^+ \to 3_1^+$				−1.03	−0.83	–	–	−0.24	−0.40
$4_4^+ \to 3_1^+$					0.04	–	–	1.38	1.56
$2_4^+ \to 2_3^+$					0.75	–	–	0.0001	−0.0002

[a] The theoretical model descriptions are given in Section 9.

[b] Harmonic vibrator.

inband transitions are positive. The same sign have been chosen for E2 matrix element for $2_2^+ \Rightarrow 3_1^+$ transition. The sign convention for the interband ME was selected by choosing negative signs for the $2_g^+ - 0_2^+$, $2_g^+ - 0_3^+$, and $2_g^+ - 2_2^+$ E2 matrix elements while a positive sign was selected for the $2_3^+ - 4_4^+$ E2 matrix element. The signs for the remaining ME were determined according to this convention, relative to those fixed ones. However, the signs of diagonal ME are observables which do not depend on convention. The present data are sensitive to the product of matrix elements $P_4 = M(0_g^+ - 2_g^+)M(2_g^+ - 2_g^+)M(2_g^+ - 2_2^+)M(2_2^+ - 0_g^+)$. Earlier Coulomb excitation work [20] determined the sign of P_4 to be negative which is consistent with the present work.

The signs were verified by performing minimization starting from different initial values and comparing the quality of fit. The overall influence of changing signs can be judged by total χ^2 at the minimum and traced to individual data points. As an example:

(a) *Negative sign of* $\langle 4_2^+ \Vert E2 \Vert 4_2^+ \rangle$ *matrix element.* χ^2 value originated from $4_2^+ \to 2_2^+$, $4_2^+ \to 4_g^+$, $4_2^+ \to 2_g^+$ gamma yields on ^{208}Pb beam and $4_2^+ \to 2_g^+$ on ^{58}Ni beam was 5.9 for negative sign and 13.5 for positive one.

(b) *Positive sign of* $\langle 2_2^+ \Vert E2 \Vert 2_2^+ \rangle$ *matrix element.* χ^2 value originated from $2_2^+ \to 0_g^+$ and $2_2^+ \to 2_g^+$ gamma yields on ^{208}Pb and ^{58}Ni beams was 8 for positive sign and 129 for negative one.

7. Results

The final set of matrix elements was obtained by making a least-squares fit to 213 data including the present Coulomb excitation yields plus the previously measured E2 moment of the 2_g^+ state, branching ratios and the E2/M1 mixing ratio. The minimum of χ^2 normalised by the number of data points is equal 1.32, which is reasonable. It was possible to determine the absolute values, as well as many of the signs, of E2 and M1 reduced matrix elements with sufficient accuracy for a meaningful comparison with theory.

The measured diagonal and off-diagonal E2 reduced matrix elements are listed in Tables 1 and 2, respectively. The reduced matrix elements $\langle I_s \Vert E2 \Vert I_r \rangle$ are defined by Eq. (1) in the next section. The measured M1 reduced matrix elements are given in Table 3.

The present results are in good agreement with prior results [3]. The only notable discrepancy is with the $B(E2; 0_2^+ \to 2_g^+)$ deduced by McGowan et al. [21], which is due to the fact that the large $B(E2; 0_2^+ \to 2_3^+)$ was not included in the Coulomb excitation analysis of [21]. Note that in some cases, such as the diagonal E2 moment of the 2_g^+ state, the final quoted error is

Table 3
Experimental M1 reduced matrix elements in μ_N units

Transition	Matrix element $\langle f\|\mathrm{M1}\|i\rangle\mu_N$
$2_g^+ \to 3_1^+$	−0.054(9)
$2_g^+ \to 2_2^+$	< 0.02
$2_g^+ \to 2_3^+$	0.24(3)
$4_g^+ \to 4_2^+$	−0.15(3)

larger than the error on the quadrupole moment value included in the fitted data set. This is due to the conservative error estimation used for the present analysis. In the experimental analysis of COULEX results the data from GSI experiments ([2] and [3]) were not taken into account. Our results for diagonal matrix elements (ME) in ground state band are in agreement to [3] data within one standard deviation. Using various projectiles we were able to get diagonal ME for 3 levels of 2_2^+ band as well as 2_3^+ state. The transitional ME are mostly the same as given in [2] and [3] within one standard deviation, few of them within two standard deviations. Having well established level scheme of 0_2^+ band we were able to get more informations about ME for intraband as well as interband transitions for the band.

The present work has determined the large set of E2 matrix elements interconnecting the lowest 17 states in ^{104}Ru. The extent of this data set is too large to discuss each matrix element in detail. The discussion of the overall implications of these results is given in Section 9.

8. Sum rules and experimental quadrupole invariants

Quadrupole collectivity produces strong correlations of the E2 matrix elements and the number of significant collective variables is much lower than the number of matrix elements [1]. Comparing list of experimental E2 matrix elements with model values exhibits neither the uniqueness nor the sensitivity of the data to the collective model parameters. Considerably better insight is obtained comparing the same charge deformation parameters from the data and with appropriate values from the model calculations, since it shows clearly which collective parameters are determined by the data and the goodness of collective model descriptions. The information about charge deformation parameters can be obtained using rotationaly invariant products of the quadrupole operators that relate the reduced E2 matrix elements with the quadrupole deformation parameters [1,5,6].

The reduced matrix elements, $\langle I_s\|\mathrm{E2}\|I_r\rangle$, of the electric quadrupole operator $\mathcal{M}(\mathrm{E2},\mu)$ ($\mu = -2,\ldots,2$), which have been discussed in the previous section, are defined as follows:

$$\langle I_s M_s|\mathcal{M}(\mathrm{E2},\mu)|I_r M_r\rangle = (-1)^{I_s-M_s}\begin{pmatrix} I_s & 2 & I_r \\ -M_s & \mu & M_r\end{pmatrix}\langle I_s\|\mathcal{M}(\mathrm{E2})\|I_r\rangle, \tag{1}$$

where the 2×3 matrix is the Wigner $3jm$ symbol. To shorten the notation we used in fact in the previous section an abbreviated form of the quadrupole operator within reduced matrix elements: $\langle I_s\|\mathcal{M}(\mathrm{E2})\|I_r\rangle = \langle I_s\|\mathrm{E2}\|I_r\rangle$. The above notation will be used also in the following.

The two basic quadrupole invariant operators are formed of the quadrupole tensor $\mathcal{M}(\mathrm{E2})$ in the following way:

$$\big[\mathcal{M}(\mathrm{E2})\times\mathcal{M}(\mathrm{E2})\big]_0 = \frac{1}{\sqrt{5}}Q^2, \tag{2}$$

$$\left[\left[\mathcal{M}(\mathrm{E2}) \times \mathcal{M}(E2)\right]_2 \times \mathcal{M}(\mathrm{E2})\right]_0 = -\sqrt{\frac{2}{35}}\, Q^3 \cos 3\delta, \tag{3}$$

where $[\cdots \times \cdots]_L$ stands for the vector coupling to angular momentum L. The coefficients in front of Q^2 and Q^3 in Eqs. (2) and (3) are the corresponding products of the Wigner symbols. These invariants are denoted here up to coefficients as Q^2 and $Q^3 \cos 3\delta$, respectively in order to have a correspondence with collective coordinates (see the next section). Since the components of $\mathcal{M}(\mathrm{E2}, \mu)$ with different μ's commute with each other the expectation values of the E2 invariants can be related to the reduced E2 matrix elements by making intermediate state expansions. The corresponding sum rules read:

$$\langle S|\left[\mathcal{M}(\mathrm{E2}) \times \mathcal{M}(\mathrm{E2})\right]_0|S\rangle = \frac{(-1)^{2S}}{\sqrt{2S+1}} \sum_R \langle S\|\mathrm{E2}\|R\rangle\langle R\|\mathrm{E2}\|S\rangle \begin{Bmatrix} 2 & 2 & 0 \\ S & S & R \end{Bmatrix}, \tag{4}$$

$$\langle S|\left[\left[\mathcal{M}(\mathrm{E2}) \times \mathcal{M}(\mathrm{E2})\right]_2 \times \mathcal{M}(\mathrm{E2})\right]_0|S\rangle = \sqrt{\frac{5}{2S+1}} \sum_{RT} \langle S\|\mathrm{E2}\|R\rangle\langle R\|\mathrm{E2}\|T\rangle\langle T\|\mathrm{E2}\|S\rangle \begin{Bmatrix} 2 & 2 & 0 \\ S & S & T \end{Bmatrix} \begin{Bmatrix} 2 & 2 & 2 \\ T & S & R \end{Bmatrix} (-1)^{3S+T}, \tag{5}$$

where S denotes state S and at the same time the spin of state S alone; R and T denotes intermediate states and their spins; $\left\{ \begin{smallmatrix} A & B & C \\ D & E & F \end{smallmatrix} \right\}$ is a $6j$ symbol. Thus, having the experimental values of the reduced E2 matrix elements, the expectation values of the basic quadrupole invariants for a given state S can be extracted from the experimental data. In a similar way the expectation values of all the rotationally invariant products of the E2 operator can be evaluated, determining directly the quantum distribution i.e., the centroids, dispersions, skewnesses, cross-correlation coefficients, etc., of $\mathcal{M}(\mathrm{E2})$ in a given state. As an example of contribution of various matrix elements to the value of the invariant in ^{104}Ru, in Tables 4 and 5 main contributions of the experimental sums (4) and (5) for $\langle 2_2^+|Q^2|2_2^+\rangle$ and $\langle 2_2^+|Q^3 \cos 3\delta|2_2^+\rangle$, respectively, are presented. One can see that only four matrix elements are crucial for both invariants. The invariant $\langle S|Q^2|S\rangle$, which is to be denoted in short as $\langle Q^2\rangle$, does not depend on sign of any matrix element, in contrast to the $\langle Q^3 \cos 3\delta\rangle$ invariant. The sign of $\langle 3_1^+\|\mathrm{E2}\|4_2^+\rangle$ matrix element was not experimentaly determined (c.f. Table 2). When the sign of $\langle 3_1^+\|\mathrm{E2}\|4_2^+\rangle$ is changed from negative to positive, then the expectation value of $\langle 2_2^+|Q^3 \cos 3\delta|2_2^+\rangle$ decreases from 0.34(8) $\mathrm{e}^3\mathrm{b}^3$ to 0.03(9) $\mathrm{e}^3\mathrm{b}^3$. Theoretical calculations within the quadrupole collective Bohr Hamiltonian and the asymmetric rigid rotor model, discussed in Section 9 below, support the negative sign. Therefore, at the further analysis, the negative sign has been accepted. The similar case is for 3_1^+ level. When $\langle 3_1^+\|E2\|4_2^+\rangle$ is negative, then $\langle 3_1^+|Q^3 \cos 3\delta|3_1^+\rangle = 0.25(^{+10}_{-8})$ $\mathrm{e}^3\mathrm{b}^3$, and when positive it will drop to 0.01(4) $\mathrm{e}^3\mathrm{b}^3$.

Although the technique of using rotational invariants has been discussed in the context of its application to the collective model, the method is completely model independent and is applicable to any spherical tensor operator. The invariants are extracted from the experimental matrix elements and thus they are equivalent to observables. They can be compared to the theoretical values obtained from collective model calculations. This way the usefulness of a given model to describing the nuclear collective states can be verified. The significance and usefulness of presenting the experimental data in the form of model-independent invariants depend on degree to which the nuclear properties are correlated by collective degrees of freedom. The recent advances in the field of Coulomb excitation make possible to determine all the E2 matrix elements required to apply this model-independent method and thereby express a wealth of data in a form that exhibits clearly the extent to which the data are correlated by collectivity. The rotational invariants

Table 4
Contribution of various matrix elements to the final result for $\langle 2_2^+|Q^2|2_2^+\rangle$ invariant in ^{104}Ru

The component	Contribution to the invariant [e^2b^2]
$\langle 2_2^+\|\|E2\|\|2_g^+\rangle\langle 2_g^+\|\|E2\|\|2_2^+\rangle$	0.113
$\langle 2_2^+\|\|E2\|\|3_1^+\rangle\langle 3_1^+\|\|E2\|\|2_2^+\rangle$	0.298
$\langle 2_2^+\|\|E2\|\|4_2^+\rangle\langle 4_2^+\|\|E2\|\|2_2^+\rangle$	0.251
$\langle 2_2^+\|\|E2\|\|2_2^+\rangle\langle 2_2^+\|\|E2\|\|2_2^+\rangle$	0.077
Total of 4 contributions	= 0.739
All contributions	= 0.76(8)

Table 5
Important contribution of matrix elements to the final result for $\langle 2_2^+|Q^3\cos 3\delta|2_2^+\rangle$ invariant in ^{104}Ru

The component	Contributions to the invariant [e^3b^3]
$\langle 2_2^+\|\|E2\|\|3_1^+\rangle\langle 3_1^+\|\|E2\|\|2_2^+\rangle\langle 2_2^+\|\|E2\|\|2_2^+\rangle$	0.176
$\langle 2_2^+\|\|E2\|\|3_1^+\rangle\langle 3_1^+\|\|E2\|\|4_2^+\rangle\langle 4_2^+\|\|E2\|\|2_2^+\rangle$	0.157
$\langle 2_2^+\|\|E2\|\|2_2^+\rangle\langle 2_2^+\|\|E2\|\|4_2^+\rangle\langle 4_2^+\|\|E2\|\|2_2^+\rangle$	−0.074
$\langle 2_2^+\|\|E2\|\|4_2^+\rangle\langle 4_2^+\|\|E2\|\|4_2^+\rangle\langle 4_2^+\|\|E2\|\|2_2^+\rangle$	0.068
Total of 4 contributions	= 0.327
All contributions	= 0.34(8)

provide the most insight into the underlying collective correlations at the expense of some loss in precision due to incomplete summation. Parameters of models selected to have reasonable values of the rotational invariants, can be fitted to the individual matrix elements, providing a more quantative comparison with the data. The rotational invariants are most valuable for studies of shape-transitional nuclei such as ^{104}Ru. Experimentally, the summations are insufficiently complete for non-collective nuclei and insufficiently precise for useful interpretations of strongly deformed rotors.

The calculation of the rotational invariants from the measured matrix elements is straightforward but estimation of the errors is difficult due to the strong cross-correlation in the errors of the matrix elements extracted from Coulomb excitation data. In many cases functions of the matrix elements defining the invariants are determined by the experimental data more accurately than the matrix elements themselves, therefore it is not possible to use the quoted errors ascribed to the individual matrix elements without including the cross-correlation effects. The errors ascribed to the invariants were obtained directly from the Coulomb excitation data by the same procedure used for estimating the errors in the individual matrix elements.

Fig. 4 shows the centroid and dispersion of the invariant Q^2 for the individual states calculated by means of the sum rules from the experimental E2 matrix elements. In the calculation, particularly for 2_2 band, the GSI data for matrix elements coupling the 3_1^+ state were used, as being more precise than the present ones.

The dispersion of Q^2 is defined by means of $\langle Q^4\rangle$ value as follows:

$$\sigma\left(Q^2\right) = \sqrt{\left\langle Q^4\right\rangle - \left\langle Q^2\right\rangle^2}.$$

For illustration we shall convert the mean values of Q^2 to the root mean square values of the shape deformation parameter β, $\beta_0 = \sqrt{\langle\beta^2\rangle}$ using formulas (A.1) and (A.2) of Appendix A.

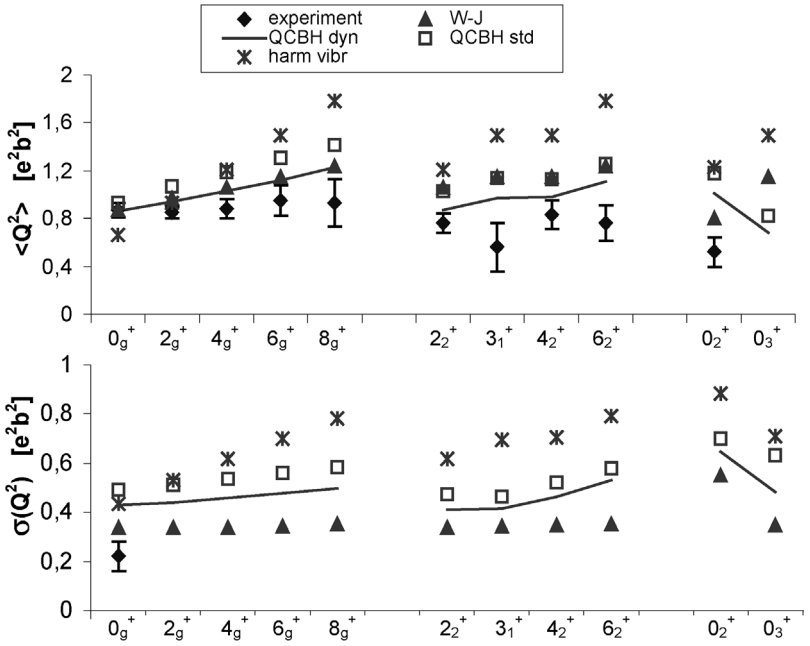

Fig. 4. Experimental and theoretical expectation values of Q^2 and dispersions $\sigma(Q^2)$ defined in the text versus spin for the ground state band, 2_2^+ band and 0_2^+ band head.

The centroids show strong correlations from state to state consistent with the band structure presented in Fig. 2. In addition, there appears to be a smooth variation in the magnitude of the quadrupole collectivity with spin value in both collective bands. Thus the expectation values of $\langle Q^2\rangle$ for the ground band are constant up to 8_g^+ level on the value about 0.9 (eb)^2 ($\beta_0 \approx 0.28$). Close and still constant along the band, a value of $\langle Q^2\rangle \approx 0.75$ (eb)^2 ($\beta_0 \approx 0.26$) is found for the 2_2^+ band. The band head of the 0_2^+ band has a still lower value of $\langle Q^2\rangle = 0.52(12)$ (eb)^2 ($\beta_0 \approx 0.21$). For ^{104}Ru low spin levels the distribution width $\sigma(Q^2) \approx 0.22(6)$, indicating modest dispersion of Q^2. The data are insufficient to provide reliable values for $\sigma(Q^2)$ for each level separately.

In the present paper we define the quadrupole asymmetry, which is a measure of deviation from the axial symmetry, in the following way:

$$\alpha(\cos 3\delta) = \langle Q^3 \cos 3\delta\rangle / \left(\langle Q^2\rangle\right)^{3/2}. \tag{6}$$

Sometimes $\alpha(\cos 3\delta)$ is defined with $\sqrt{\langle Q^2\rangle\langle Q^4\rangle}$ in denominator instead of $(\langle Q^2\rangle)^{3/2}$. In Ref. [1] and other papers of our collaborations the quantity $\alpha(\cos 3\delta)$ was denoted as $\langle\cos 3\delta\rangle$ although the value of $\langle\cos 3\delta\rangle$ is not precisely the quantity at the right-hand side of Eq. (6).

In analogy to β_0, we introduce a measure of the shape deformation parameter γ in a given state by $\gamma_0 = \frac{1}{3}\arccos(\alpha(\cos 3\gamma))$ using again the formulas (A.1) and (A.2) of Appendix A.

We define the dispersion of the quadrupole asymmetry as follows:

$$\sigma\left(\alpha(\cos 3\delta)\right) = \sqrt{\frac{\langle Q^6 \cos^2 3\delta\rangle}{\langle Q^6\rangle} - \left(\alpha(\cos 3\delta)\right)^2}. \tag{7}$$

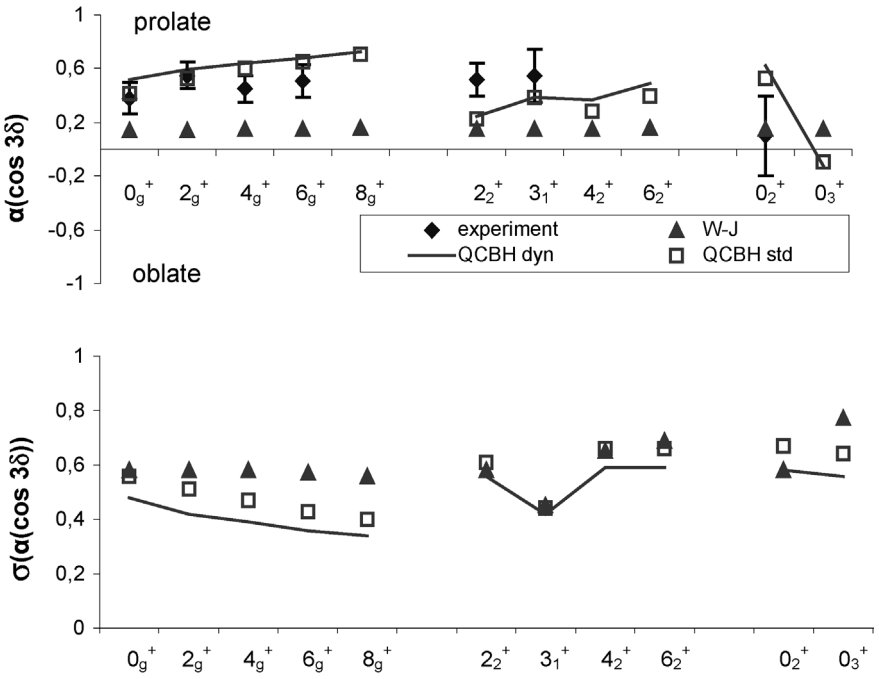

Fig. 5. Experimental and theoretical values of the quadrupole asymmetry and the dispersions of quadrupole asymmetry versus spin for the ground state band, 2_2^+ band and 0_2^+ band head. Both quantities are defined by Eqs. (6) and (7).

The quadrupole asymmetry is also correlated from state to state in each 'quasi' band. The value of $\alpha(\cos 3\delta)$ is lower than 0.40 for the ground level and grows to more than 0.45 for higher levels of the band (it corresponds to $\gamma_0 \approx 25°$ and 23°, respectively). The value of $\alpha(\cos 3\delta)$ for the 2_2^+ band and 0_2^+ state is equal to about 0.5 and 0.1(3) what is equivalent to $\gamma_0 \approx 22°$ and 30°, respectively. For relating $\langle Q^2 \rangle$ and $\langle Q^3 \cos 3\delta \rangle$ to the corresponding quantities dependent on β and γ formulas (A.1) and (A.2) of Appendix A have been applied. Thus, the asymmetry values indicate predominantly prolate triaxial shape for all bands. The information regarding the dispersion of the quadrupole asymmetry is less complete and gives only a guess that the ^{104}Ru nuclei is soft for γ deformation.

Concluding, the experimental data are consistent with quadrupole collectivity with modest softness in magnitude of Q. The experimental values of $\sigma(\alpha(\cos 3\delta))$ are not quoted because of possible incompleteness in evaluating higher order invariants. Thus the degree of the γ-softness can be concluded only from a model predictions.

9. Comparison with theoretical model calculations

Analysis of the present data, using rotational invariants, shows that the E2 properties of ^{104}Ru are well correlated with macroscopic quadrupole collective degrees of freedom. The experimental results suggest that ^{104}Ru is triaxially deformed and modestly soft in the β degree of freedom. In this section a comparison with various quadrupole collective models based on the generalized Bohr Hamiltonian [22,23] will be given:

$$\mathcal{H}_{\mathrm{QC}} = \mathcal{T}_{\mathrm{vib}}(\beta, \gamma) + \mathcal{T}_{\mathrm{rot}}(\beta, \gamma, \Omega) + \mathcal{V}_{\mathrm{def}}(\beta, \gamma), \tag{8}$$

where the dynamical variables β, γ and Ω are the two Bohr shape deformation parameters and the three Euler angles, respectively; $\mathcal{V}_{\rm def}$ is the quadrupole deformation potential,

$$\mathcal{T}_{\rm vib} = -\frac{\hbar^2}{2\sqrt{\mathcal{W}\mathcal{R}}}\left\{\frac{1}{\beta^4}\left[\partial_\beta\left(\beta^4\sqrt{\frac{\mathcal{R}}{\mathcal{W}}}\mathcal{B}_{\gamma\gamma}\partial_\beta\right) - \partial_\beta\left(\beta^3\sqrt{\frac{\mathcal{R}}{\mathcal{W}}}\mathcal{B}_{\beta\gamma}\partial_\gamma\right)\right]\right.$$
$$\left. + \frac{1}{\beta\sin 3\gamma}\left[-\partial_\gamma\left(\sqrt{\frac{\mathcal{R}}{\mathcal{W}}}\sin 3\gamma\,\mathcal{B}_{\beta\gamma}\partial_\beta\right) + \frac{1}{\beta}\partial_\gamma\left(\sqrt{\frac{\mathcal{R}}{\mathcal{W}}}\sin 3\gamma\,\mathcal{B}_{\beta\beta}\right)\partial_\gamma\right]\right\} \tag{9}$$

with $\mathcal{W} = \mathcal{B}_{\beta\beta}\mathcal{B}_{\gamma\gamma} - \mathcal{B}_{\beta\gamma}$, $\mathcal{R} = \mathcal{B}_x\mathcal{B}_y\mathcal{B}_z$ and

$$\mathcal{T}_{\rm rot} = \frac{1}{8\beta^2}\sum_{\kappa=x,y,z} I_\kappa^2(\Omega)/\big(\mathcal{B}_\kappa(\beta,\gamma)\sin^2\gamma_\kappa\big), \tag{10}$$

with $\gamma_x = \gamma - 2\pi/3$, $\gamma_y = \gamma + 2\pi/3$, $\gamma_z = \gamma$ are the collective vibrational and rotational kinetic energies, respectively. The differential operators in Ω, I_x, I_y, I_z are the intrinsic components of the total angular momentum. The Hamiltonian (8) is defined by the seven functions of β and γ: $\mathcal{V}$, the potential, and $\mathcal{B}_{\beta\beta}$, $\mathcal{B}_{\beta\gamma}$, $\mathcal{B}_{\gamma\gamma}$ and $\mathcal{B}_x$, $\mathcal{B}_y$, $\mathcal{B}_z$, the vibrational and rotational inertial functions, respectively. In order to calculate electromagnetic transitions also collective multipole operators are defined. In the collective model the E2 operator, $\mathcal{M}(\mathrm{E2},\mu)$, forms a quadrupole tensor dependent on the all colective coordinates: deformations β and γ, and the Euler angles. It is fully determined by its two non-vanishing intrinsic components, $Q_0(\beta,\gamma) = \mathcal{M}(\mathrm{E2},0)$ and $Q_2(\beta,\gamma) = \sqrt{2}\mathcal{M}(\mathrm{E2},2)$ being functions of the deformations only.

First, the experimental data will be compared to the calculations performed with the Bohr Hamiltonian which is determined from a microscopic theory (QCBH) with no free parameters [11]. Next the comparison will be made to simple phenomenological models being a symmetry limits of collective Bohr Hamiltonian: the beta- and gamma-rigid Davydov–Filippov model (D–F), and the gamma-unstable Wilets–Jean model (W–J), both with parameters fitted to the experimental data.

When comparing the model results with data we are focusing on the quadrupole invariants (see [1]) that allow for a determination of nuclear intrinsic shapes in a model independent way. The analysis in terms of quadrupole invariants is based on specific sum rules (see Section 8), which involve summations over a large set of quadrupole matrix elements. An essential element of such an analysis is the fact that the components of the quadrupole-moment operator commute [10]; as is obviously the case for the microscopic quadrupole moment, which depends only on coordinates of particles. This feature of the quadrupole operator is preserved in the collective models used below, where the quadrupole operator depends only on collective coordinates; and thus its components do commute. On the other hand, such a property is absent in a truncated shell-model approach, or in an approximation thereof such as, e.g., the IBM, where the components of the quadrupole-moment operator do not commute. This is particularly well visible within the IBM, where a simple phenomenological approximation of the quadrupole moment in the truncated space is postulated with parameters fit to data. Such an approximation usually gives a correct description of selected experimental matrix elements, see [7–9] for application to ^{104}Ru. However, when the whole set of matrix elements is considered, as is the case for the sum-rule analysis, non-commutativity of the model quadrupole moment violates the microscopic sum rules [10]. For this reason, one cannot perform such an analysis in a truncated shell model or IBM. One can say that the reason for that is the fact that within the whole set of quadrupole matrix elements there must

be some or many, for which a substantial strength is certainly located outside the truncated space.

Below we first recapitulate briefly the models used to the comparison.

9.1. Microscopic quadrupole collective Bohr Hamiltonian (QCBH)

Prediction of the thirty E2 matrix elements measured in the present experiments poses a challenge to general quadrupole collective calculations. Such a calculation has been undertaken in paper [11]. The starting point to this calculation is a microscopic Hamiltonian

$$H = H_{\text{Nilsson}}(\beta, \gamma) + V_{\text{pairing}} \tag{11}$$

representing the system of nucleons in a deformed triaxial Nilsson potential well interacting through the standard pairing forces. Thus, β and γ are defined here as the Bohr shape deformation parameters of a triaxial harmonic oscillator potential well with frequencies

$$\omega_\kappa(\beta, \gamma) = \omega_0(\beta, \gamma)\left(1 + \sqrt{\frac{5}{4\pi}}\beta\cos\gamma_\kappa\right)^{-1} = \omega_0(\beta, \gamma)(1 + 4C\beta\cos\gamma_\kappa)^{-1}, \tag{12}$$

where $C = (1/4)\sqrt{5/4\pi}$ and

$$\omega_0(\beta, \gamma) = \mathring{\omega}_0\big(1 - 12C^2\beta^2 + 16C^3\beta^3\cos 3\gamma\big)^{1/3}, \tag{13}$$

for $\kappa = x, y, z$ [25]. For years the standard approach to a microscopic determination of the collective model for the quadrupole excitations has been to assume that the only dynamical variables are the quadrupole deformations β and γ, and the Euler angles Ω and then extracting the collective Hamiltonian $\mathcal{H}_{\text{QC}}$ of Eq. (8) from a microscopic Hamiltonian H of Eq. (11). In Ref. [11] the standard cranking method to evaluate the inertial functions and the macroscopic-microscopic method to evaluate the potential has been used. Below, we refer to that method of calculation as the standard quadrupole collective Bohr Hamiltonian approach (QCBH_{std}). A new approach developed in ref. [11] lies in extending the space of collective variables. In addition to the quadrupole variables four others are introduced which are connected with the proton and neutron collective pairing vibrations and rotations (i.e., collective pair transfers), namely, Δ_p and Δ_n, the proton and neutron energy gaps, and Φ_p and Φ_n, the proton and neutron gauge angles, respectively. Then, a general collective "quadrupole + pairing" Hamiltonian extracted from microscopic Hamiltonian H takes the following form:

$$\mathcal{H}_{\text{QPC}} = \mathcal{H}_{\text{QC}} + \mathcal{H}_{\text{PC}} + \mathcal{T}_{\text{QP}}. \tag{14}$$

The first term $\mathcal{H}_{\text{QC}}$ describes the collective quadrupole vibrations and rotations and has the form of that of Eq. (8). The second term in (14) is a sum of the pairing collective Hamiltonians for protons and neutrons determined by the two vibrational functions, $\mathcal{B}_{\Delta_p\Delta_p}$ and $\mathcal{B}_{\Delta_n\Delta_n}$, the two "moments of inertia", $\mathcal{I}_{\Phi_p}$ and $\mathcal{I}_{\Phi_n}$, and the two pairing potentials, $\mathcal{V}_p$ and $\mathcal{V}_n$ for the proton and the neutron pairing vibrations and rotations, respectively. All these functions are determined microscopically. The third term in (14), $\mathcal{T}_{\text{QP}}$, represents a quadrupole-pairing coupling in the collective kinetic energy and contains another four inertial functions, $\mathcal{B}_{\beta\Delta_p}$, $\mathcal{B}_{\gamma\Delta_p}$, $\mathcal{B}_{\beta\Delta_n}$ and $\mathcal{B}_{\gamma\Delta_n}$, which describe a coupling of the β- and the γ-vibrations to the proton and neutron pairing vibrations, respectively, in the kinetic energy. In general, all the functions involved in Hamiltonian $\mathcal{H}_{\text{QPC}}$ of Eq. (14) depend on β, γ, Δ_p and Δ_n. The intrinsic quadrupole moments, Q_0 and Q_2 can be calculated from the microscopic theory in a similar way.

The Born–Oppenheimer approximation to the Hamiltonian $\mathcal{H}_{\mathrm{QPC}}$ has been used to investigate the quadrupole collective excitations. This means that $\mathcal{T}_{\mathrm{QP}}$ is neglected and first the ground state of Hamiltonian $\mathcal{H}_{\mathrm{PC}}$ is found for given β and γ. Next, the most probable values of Δ_p and Δ_n, which depend on β and γ, in the ground state of the pairing vibrations are put into the Bohr Hamiltonian $\mathcal{H}_{\mathrm{QC}}$. Finally, that Bohr Hamiltonian is diagonalized. This way the effect of the zero-point pairing proton and neutron vibrations on the quadrupole vibrations is taken into account and found to be an essential effect. We refer to the above method of investigation of the quadrupole excitations as the dynamical quadrupole collective Bohr Hamiltonian ($\mathrm{QCBH_{dyn}}$).

The results of calculations using both of the above methods of constructing the Bohr Hamiltonian microscopically are given in Tables 1 and 2 and on Figs. 6–10. Neither calculation contains parameters fit to the ^{104}Ru experimental data. The agreement between the $\mathrm{QCBH_{dyn}}$ calculations and experiment is good in spite of the fact that no free parameters have been fit. The $\mathrm{QCBH_{std}}$ calculations are not as successful, particularly the levels energy predictions.

9.2. The Davydov–Filippov model (D–F)

Expectation value of the invariant $Q^3\cos 3\delta$ indicate appreciable triaxiality of ^{104}Ru in the ground and excited states. The simplest symmetry limit model describing triaxiality of nuclei is the rigid triaxial rotor model of Davydov–Filippov [24]. In this model the Hamiltonian (8) is limited only to the rotational kinetic energy part, $\mathcal{T}_{\mathrm{rot}}$ (see (10)) with

$$\mathcal{B}_x = \mathcal{B}_y = \mathcal{B}_z = B = \mathrm{const} \tag{15}$$

and the only dynamical variables are the Euler angles; $\beta = \beta_0$ and $\gamma = \gamma_0$ become fixed deformation parameters. Three phenomenological parameters B, β_0, γ_0 are adjusted to experimental data. Instead of the parameter B, the energy of the first 2^+ level, E_{2^+} is used. In Davydov–Filippov model E_{2^+} is a simple function of B, β_0 and γ_0. The results of the calculation for $E_{2^+} = 320$ keV, $\beta_0 = 0.28$ and $\gamma_0 = 25^\circ$ are shown in Figs. 6–10 and Tables 1 and 2. One can see (Fig. 6) that the spectrum calculated by the Davydov–Filippov model is much more stretched than the experimental one.

9.3. The Wilets–Jean model (W–J)

The other symmetry limit of the quadrupole collective Hamiltonian (8) describing triaxiality is the Wilets–Jean model [26] of γ-unstable deformation i.e., gamma-independent collective potential. In the present paper, it will be used in the extended form proposed in [27]. The collective potential then reads

$$\mathcal{V}_{\mathrm{coll}}(\beta,\gamma) = V(\beta) = \frac{1}{2}C\beta^2 + G\big(e^{-(\frac{\beta}{\alpha})^2} - 1\big). \tag{16}$$

All inertial functions are assumed to be β and γ independent:

$$\mathcal{B}_{\gamma\gamma} = \mathcal{B}_x = \mathcal{B}_y = \mathcal{B}_z = B = \mathrm{const}, \qquad \mathcal{B}_{\beta\beta} = \mathrm{const}, \qquad B_{\beta\gamma} = 0. \tag{17}$$

Fig. 11 shows the pattern of energy levels predicted by the model. There are two quantum numbers: λ, the seniority and n_β, the number of nodes in the β-dependent part of the wave func-

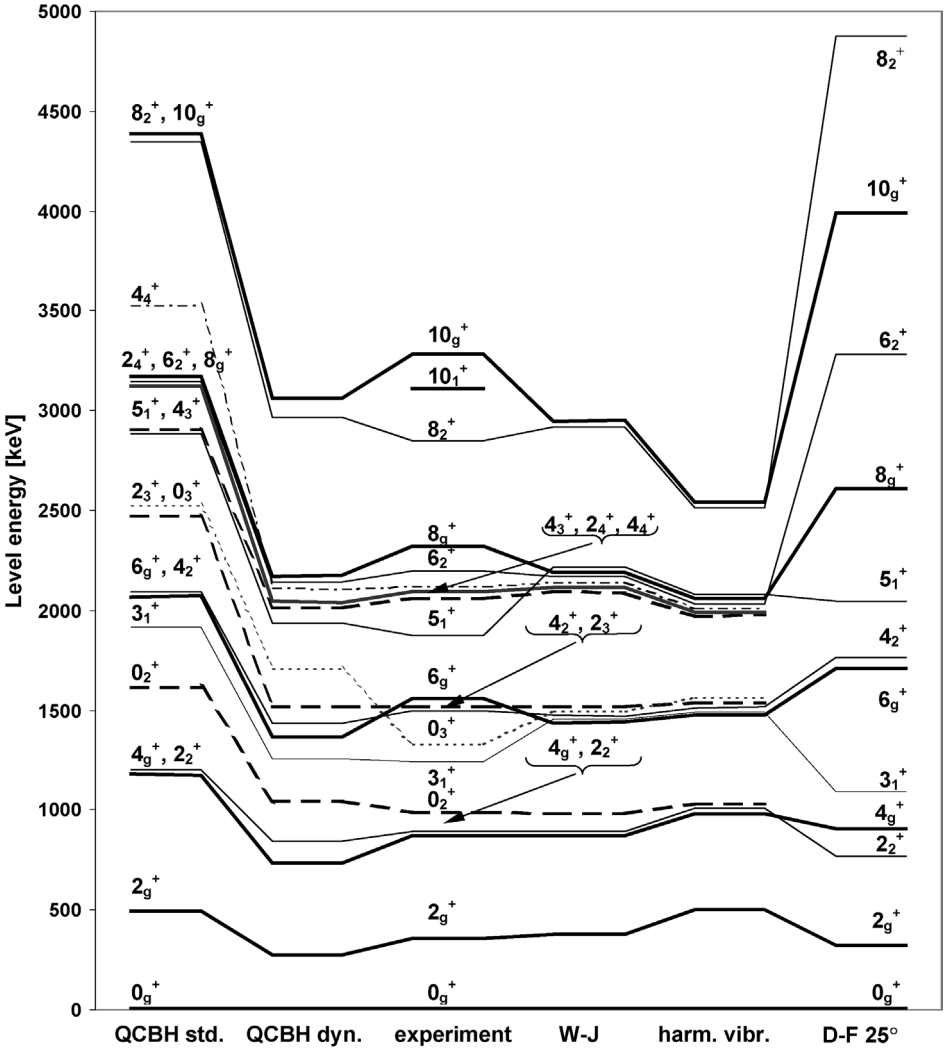

Fig. 6. Comparison of experimental and theoretical energy levels values. Ground state band levels are marked by thick continous lines, 2_2^+ band levels are marked by thin continous lines, 0_2^+ band levels are marked by thick dashed lines, 0_3^+ band levels are marked by dotted lines.

tion. For $G \gg C\alpha^2/2$ the potential has its minimum at $\beta = \beta_0 \gg 0$ and the collective motion can be considered as rotations strongly coupled to γ-vibrations and one-dimensional β-vibrations around a deformed minimum. Then, the selection rules of the allowed E2 transitions are: $\Delta\lambda = 1$ and $\Delta n_\beta = 0, 1$. For $G = 0$, the minimum of the potential is $\beta_0 = 0$ and we have the standard vibrational limit of five-dimensional quadrupole vibrations around the spherical shape. Then, the principal quantum number $N = 2n_\beta + \lambda$ becomes a good quantum number and the selection rule for allowed E2 transitions is $\Delta N = 1$.

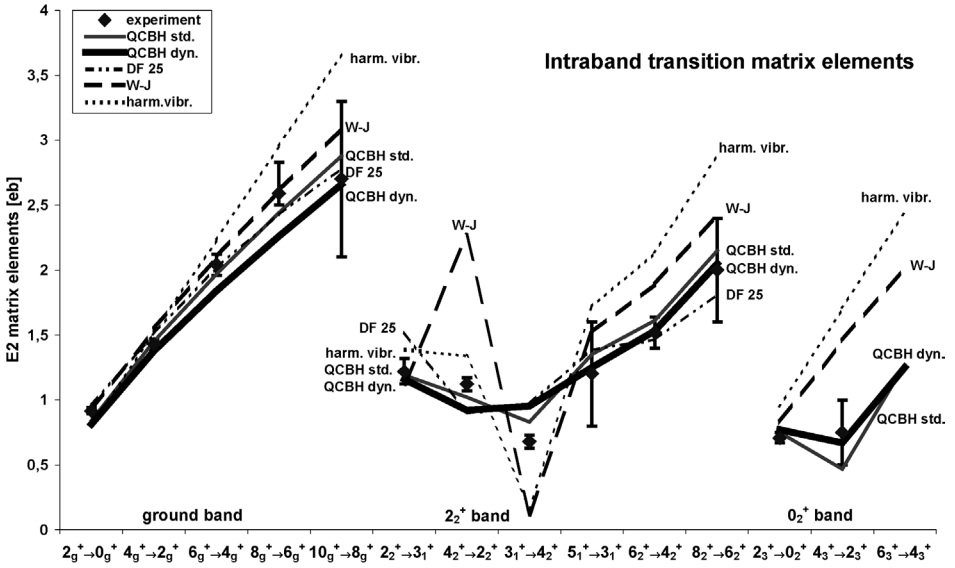

Fig. 7. Intraband transition E2 matrix elements for the ground, 2_2^+ and 0_2^+ bands.

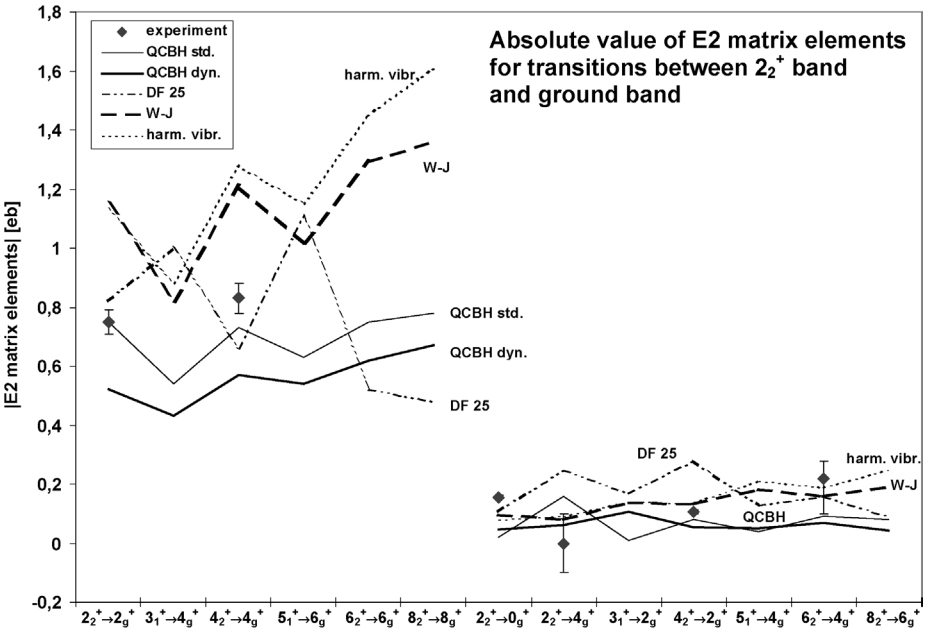

Fig. 8. Absolute value of E2 matrix elements for transitions between 2_2^+ band and ground band.

9.4. *Energy levels*

Detailed comparison of the experimental and theoretical spin, parity and energy values of ^{104}Ru levels is shown in Fig. 6. All of the experimental levels shown in Fig. 2 are included. The comparison with the predictions of the five following models is shown:

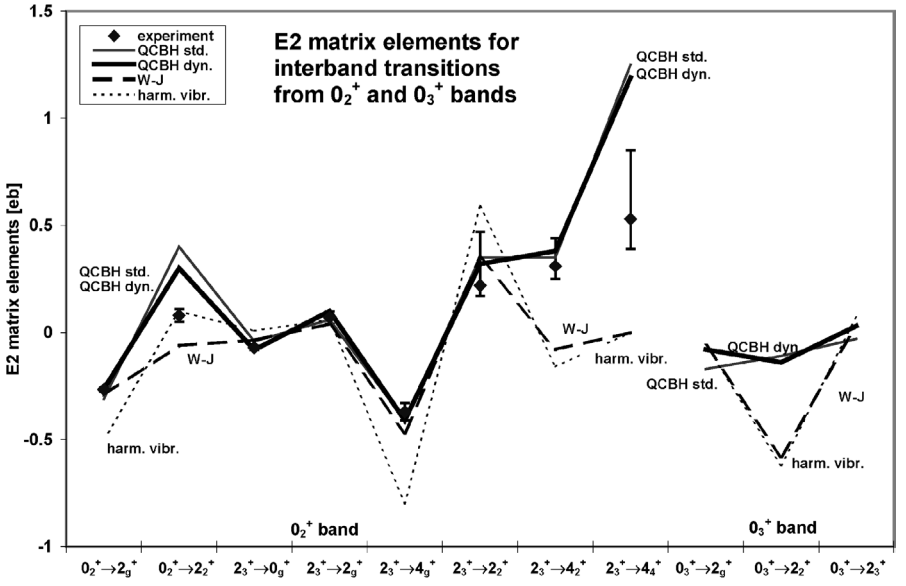

Fig. 9. E2 matrix elements for interband transitions from 0_2^+ and 0_3^+ bands.

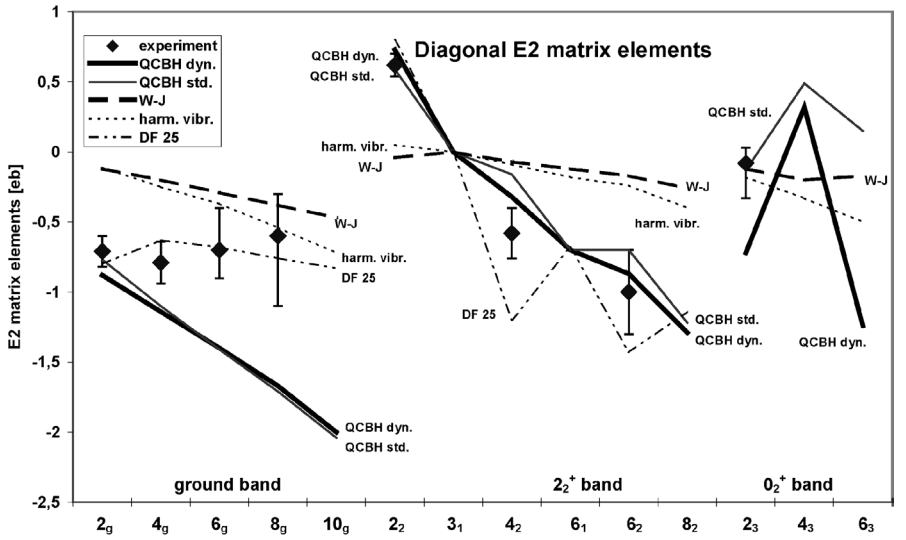

Fig. 10. Comparison of the experimental and theoretical diagonal E2 matrix elements.

(1) the standard microscopic quadrupole collective Bohr Hamiltonian—$\mathrm{QCBH_{std}}$,
(2) the microscopic quadrupole collective Bohr Hamiltonian with the effect of dynamical pairing—$\mathrm{QCBH_{dyn}}$,
(3) the rigid triaxial rotor—D–F,
(4) the γ-unstable β-vibrator in the version of Ref. [27]—W–J,
(5) the standard quadrupole harmonic vibrator—harm. vibr.

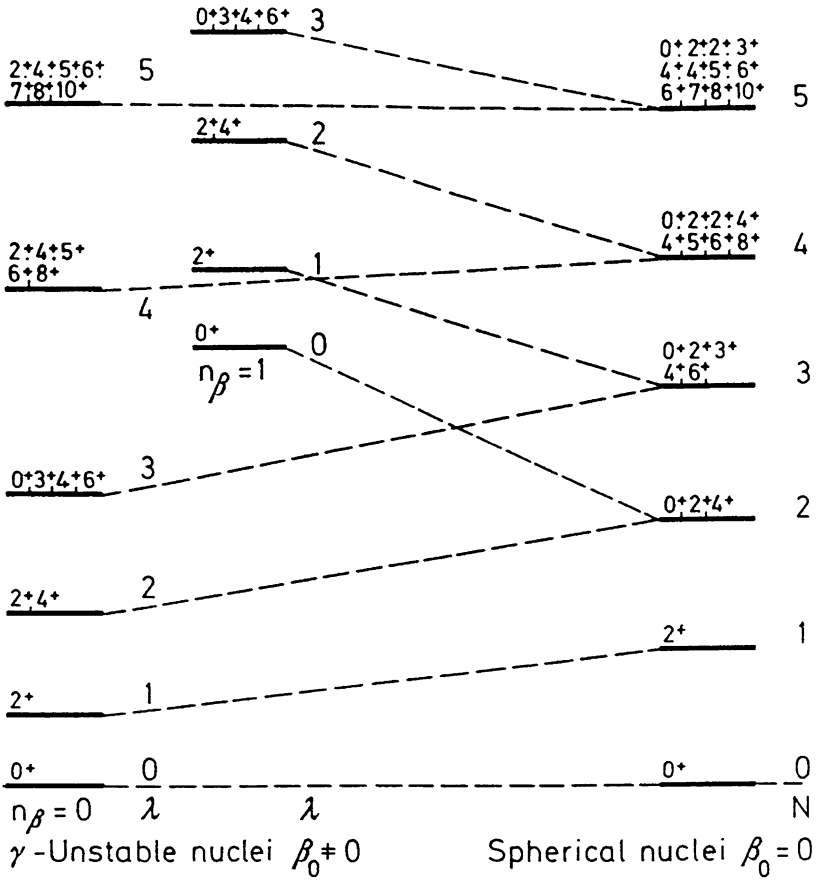

Fig. 11. The level schemes according to gamma-soft model [27] for $\beta_0 = 0$ (spherical nuclei) and for $\beta_0 \gg 0$ (γ-unstable nuclei). In case of spherical nuclei the multiplets can be labelled by the number of phonons $N = 2n_\beta + \lambda$, whereas in the case of γ-unstable nuclei the n_β and λ quantum numbers must be given separately.

When account is taken that $\mathrm{QCBH_{dyn}}$ does not use any fitted parameter, the agreement is very good. One can see (Fig. 6) that effect of the pairing dynamics is essential for reproduction of the absolute experimental energy levels. It is worth noting the similarity of the energy patterns of the $\mathrm{QCBH_{dyn}}$ and W–J model. The energy multiplets of the W–J are well reproduced in the $\mathrm{QCBH_{dyn}}$ and in the experimental data. A similar tendency can be observed in the energy level ratios of the yrast band. In Table 6 the energy ratio $\mathcal{E}_I = E_{I^+}/E_{2^+}$ are given for the ^{104}Ru experimental data and for QCBH (standard and dynamic pairing), W–J γ-soft ($\beta_0 = 0$ and $\beta_0 \gg 0$) and D–F γ-rigid ($\gamma_0 = 30°$ and $\gamma_0 = 0°$). The experimental data are very close to the W–J γ-unstable model prediction.

9.5. Electric quadrupole matrix elements

The comparison of experimental and calculated E2 matrix elements is given in Figs. 7–10. In Fig. 7 the intraband transition matrix elements are given for the ground band, 2_2^+ band and 0_2^+ band. One can see that the difference between the QCBH results with standard and dynamic

Table 6
Level energies ratio $\mathcal{E}_I = E_I/E_{2^+}$ for the ground state band according to different models and the microscopic calculations

Model	$\mathcal{E}_I$	$\mathcal{E}_4$	$\mathcal{E}_6$	$\mathcal{E}_8$	$\mathcal{E}_{10}$
Harmonic vibrations around $\beta_0 = 0$	$\frac{1}{2}I$	2	3	4	5
γ-unstable β-vibrations (W–J), $\beta_0 \gg 0$	$\frac{1}{16}I(I+6)$	2.5	4.5	7	10
Rigid triaxial rotor (D–F) with $\gamma_0 = 30°$	$\frac{1}{12}I(I+4)$	2.67	5	8	11.67
Axial rotor with $\gamma_0 = 0°$ or $\gamma_0 = 60°$	$\frac{1}{6}I(I+1)$	3.33	7	12	18.33
$\mathrm{QCBH_{std}}$		2.43	4.24	6.40	8.90
$\mathrm{QCBH_{dyn}}$		2.71	5.03	7.90	11.28
^{104}Ru experiment		2.48	4.35	6.45	9.18

pairing is very small in contrast to the case of the level energies. In Fig. 8 the interband transition matrix elements between the 2_2^+ band and ground band are shown. For the $\Delta\lambda \neq 1$ forbidden transitions within the W–J γ-unstable model all the experimental as well as theoretical values are very small and differ little between the various theoretical calculations. In Fig. 9 the E2 interband transition matrix elements are shown for γ-transitions from bands based on the 0_2^+ and 0_3^+ levels. It is clear, that the results of the QCBH with both standard and dynamic pairing are very similar. For the transitions $2_3^+ \Rightarrow 4_2^+$ and $2_3^+ \Rightarrow 4_4^+$ the W–J γ-unstable model selection rules (see Fig. 11) are violated in the experiment as well as in the QCBH calculations. For all other transitions those selection rules are valid. In Fig. 10 the diagonal E2 matrix elements are shown. For the ground state band their experimental absolute values are lower than calculated within the microscopic QCBH models. However, the difference between the QCBH calculations and experiment are within three standard deviations.

9.6. Collective quadrupole invariants

Although the intrinsic quadrupole moments, Q_0 and Q_2, can be calculated from the microscopic theory within QCBH, we assume for simplicity in all used here versions of the collective model the same collective E2 moments of an ellipsoid, charged uniformly, of deformations β and γ defined in (12) and volume $(4/3)\pi R_0^3$, $R_0 = r_0 A^{1/3}$ and $r_0 = 1.2$ fm, namely

$$Q_0(\beta,\gamma) = \frac{3}{4\pi} Z R^2 \big(\beta\cos\gamma + C\beta^2\cos 2\gamma\big), \tag{18}$$

$$Q_2(\beta,\gamma) = \frac{3}{4\pi} Z R^2 \big(\beta\sin\gamma - C\beta^2\sin 2\gamma\big), \tag{19}$$

where C is defined in Eq. (12) and

$$R(\beta,\gamma) = R_0\big(1 - 12C^2\beta^2 + 16C^3\beta^3\cos 3\gamma\big)^{-1/3}.$$

This is a good approximation for the microscopic E2 moments.

The collective quadrupole invariants can now be expressed as functions of the two charge deformation parameters, Q and δ, defined by formulae:

$$Q_0 = Q\cos\delta, \qquad Q_2 = Q\sin\delta. \tag{20}$$

They read:

$$\big[\mathcal{M}(\mathrm{E2})\times\mathcal{M}(\mathrm{E2})\big]_0 = \frac{1}{\sqrt{5}}\big(Q_0^2+Q_2^2\big)=\frac{1}{\sqrt{5}}Q^2, \tag{21}$$

$$\big[\big[\mathcal{M}(\mathrm{E2})\times\mathcal{M}(\mathrm{E2})\big]_2\times\mathcal{M}(\mathrm{E2})\big]_0 = -\sqrt{\frac{2}{35}}\big(Q_0^3-3Q_0Q_2^2\big)=-\sqrt{\frac{2}{35}}Q^3\cos 3\delta, \tag{22}$$

$$\big[\big[\mathcal{M}(\mathrm{E2})\times\mathcal{M}(\mathrm{E2})\big]_0\big[\mathcal{M}(\mathrm{E2})\times\mathcal{M}(\mathrm{E2})\big]_0\big]_0 = \frac{1}{5}\big(Q_0^4+2Q_0^2Q_2^2+Q_2^4\big)=\frac{1}{5}Q^4, \tag{23}$$

$$\big[\big[\mathcal{M}(\mathrm{E2})\times\mathcal{M}(\mathrm{E2})\big]_0\big[\big[\mathcal{M}(\mathrm{E2})\times\mathcal{M}(\mathrm{E2})\big]_2\times\mathcal{M}(\mathrm{E2})\big]_0\big]_0 = -\sqrt{\frac{2}{175}}\big(Q_0^5-2Q_0^3Q_2^2-3Q_0Q_2^4\big)=-\sqrt{\frac{2}{175}}Q^5\cos 3\delta, \tag{24}$$

$$\big[\big[\mathcal{M}(\mathrm{E2})\times\mathcal{M}(\mathrm{E2})\big]_0\big[\mathcal{M}(\mathrm{E2})\times\mathcal{M}(\mathrm{E2})\big]_0\big[\mathcal{M}(\mathrm{E2})\times\mathcal{M}(\mathrm{E2})\big]_0\big]_0 = \frac{1}{5\sqrt{5}}\big(Q_0^6+3Q_0^4Q_2^2+3Q_0^2Q_2^4+Q_2^6\big)=\frac{1}{5\sqrt{5}}Q^6, \tag{25}$$

$$\big[\big[\big[\mathcal{M}(\mathrm{E2})\times\mathcal{M}(\mathrm{E2})\big]_2\times\mathcal{M}(\mathrm{E2})\big]_0\big[\big[\mathcal{M}(\mathrm{E2})\times\mathcal{M}(\mathrm{E2})\big]_2\times\mathcal{M}(\mathrm{E2})\big]_0\big]_0 = \frac{2}{35}\big(Q_0^6-6Q_0^4Q_2^2+9Q_0^2Q_2^4\big)=\frac{2}{35}Q^6\cos^2 3\delta. \tag{26}$$

The exact and approximated formulae for the collective quadrupole invariants as functions of β and γ are given in Appendix A. The expectation values of the all above collective quadrupole invariants can be calculated using the collective wave functions. This way the theoretical expectation values of the quadrupole invariants obtained from the collective model calculations can be compared with the experimental expectation values obtain from the sum rules.

The upper plots of Figs. 4 and 5 show the experimental results for $\langle Q^2\rangle$ and $\alpha(\cos 3\delta)$ of various states together with their experimental errors. On the same plots the theoretical values of $\langle Q^2\rangle$ and $\alpha(\cos 3\delta)$ for the same states are given using wave functions calculated in the frame of the five microscopic and phenomenological collective quadrupole models, discussed previously. The lower plots of Figs. 4 and 5 show the theoretical values of the dispersions $\sigma(Q^2)$ and $\sigma(\alpha(\cos 3\delta))$ for the same states. Unfortunately, the data available do not allow for the experimental determination of dispersions $\sigma(Q^2)$ and $\sigma(\alpha(\cos 3\delta))$. Since the quadrupole operator of the geometrical model is a commutative one, its matrix elements automatically fulfill the conditions imposed by the microscopic sum rules (see [10] for details).

10. Summary

A set of twenty eight E2 and three M1 matrix elements for ^{104}Ru have been measured from Coulomb excitation experiments using ^{208}Pb, ^{136}Xe and ^{56}Ni projectiles. This set includes the magnitudes and signs of many E2 elements coupling 17 collective states, comprising four diagonal elements for the ground state band, three diagonal elements for 2_2^+ state band and one for the 2_3^+ state of the 0_2^+ band.

Such a large set of experimental E2 matrix elements allows for projecting collective degree of freedom $\langle Q^2\rangle$ and $\alpha(\cos 3\delta)$. The present work shows that for the two bands based on ground and 2_2 states the deformation is about $\beta_0\approx 0.28$ and $\gamma_0\approx 25^\circ$. The experimental E2 collective

degree of freedom $\langle Q^2 \rangle$ and $\alpha(\cos 3\delta)$ are compared with calculations in the framework of the collective quadrupole Bohr Hamiltonian. Calculations were performed with phenomenologically fitted parameters for different symmetry limits of the Bohr Hamiltonian as well as with parameters calculated microscopically within the quadrupole (Nilsson) plus pairing approach. Results of the microscopic collective model calculations, without any parameters fitted to the ^{104}Ru data, show very good agreement with the experimental data.

Acknowledgements

The authors would like to thank Jacek Dobaczewski for his permanent interest in our research and particularly for enlightening discussion on the problem of commutativity of the components of quadrupole moment operator in different approaches. Thanks are due to P. Napiórkowski and M. Zielińska for reading the manuscript and fruitful discussion. This work has been supported in part by the Polish State Committee for Scientific Research as a research project in years 2003–2005 and by the US National Science Foundation. Two of us (S.G.R. and L.P.) were supported in part by Polish State Committee for Scientific Research (KBN) under contract No. 1 P03B 059 27 and No. 2 P03B 042 27, respectively.

Appendix A. The quadrupole invariants for an uniformly charged elipsoid

From Eqs. (21) and (22) the formulae for the two basic collective quadrupole invariants are:

$$\begin{aligned} Q^2 &= \left(\frac{3}{4\pi} Z R^2\right)^2 \left(\beta^2 + 2C\beta^3 \cos 3\gamma + C^2\beta^4\right) \\ &\approx q_0^2 \left(\beta^2 + 2C\beta^3 \cos 3\gamma + 17C^2\beta^4\right) + \mathcal{O}\left(\beta^5\right), \end{aligned} \tag{A.1}$$

$$\begin{aligned} Q^3 \cos 3\delta &= \left(\frac{3}{4\pi} Z R^2\right)^3 \left(\beta^3 \cos 3\gamma + 3C\beta^4 + 3C^2\beta^5 \cos 3\gamma + 2C^3\beta^6 \cos^2 3\gamma - C^3\beta^6\right) \\ &\approx q_0^3 \left(\beta^3 \cos 3\gamma + 3C\beta^4 + 27C^2\beta^5 \cos 3\gamma - 30C^3\beta^6 \cos^2 3\gamma + 71C^3\beta^6\right) \\ &\quad + \mathcal{O}\left(\beta^7\right), \end{aligned} \tag{A.2}$$

where $q_0 = (3/4\pi) Z R_0^2$. Calculating the mean values of invariants in β and γ in a given state the mean values of the quadrupole invariants can be calculated from the above formulas. To calculate also the dispersions of these invariants their higher powers as functions of β and γ are needed. Three of them of the order up to the sixth in Q are calculated from Eqs. (23), (24) and (26) and read:

$$\begin{aligned} Q^4 &= \left(\frac{3}{4\pi} Z R^2\right)^4 \left(\beta^4 + 4C\beta^5 \cos 3\gamma + 2C^2\beta^6 \right. \\ &\quad \left. + 4C^2\beta^6 \cos^2 3\gamma + 4C^3\beta^7 \cos 3\gamma + C^4\beta^8\right) \\ &\approx q_0^4 \left(\beta^4 + 4C\beta^5 \cos 3\gamma + 34C^2\beta^6 + 4C^2\beta^6 \cos^2 3\gamma \right. \\ &\quad \left. + \frac{1}{3}\left(268C^3\beta^7 \cos 3\gamma - 128C^4\beta^8 \cos^2 3\gamma + 2307C^4\beta^8\right)\right) + \mathcal{O}\left(\beta^9\right), \end{aligned} \tag{A.3}$$

$$
\begin{aligned}
Q^5\cos 3\delta = {} & \left(\frac{3}{4\pi}ZR^2\right)^5\big(\beta^5\cos 3\gamma + 2C\beta^6\cos^2 3\gamma + 3C\beta^6 \\
& + 10C^2\beta^7\cos 3\gamma + 8C^3\beta^8\cos^2 3\gamma + 2C^3\beta^8 \\
& + 4C^4\beta^9\cos^3 3\gamma + C^4\beta^9\cos 3\gamma + 2C^5\beta^{10}\cos^2 3\gamma - C^5\beta^{10}\big) \\
\approx {} & q_0^5\bigg(\beta^5\cos 3\gamma + 2C\beta^6\cos^2 3\gamma + 3C\beta^6 \\
& + 50C^2\beta^7\cos 3\gamma + 122C^3\beta^8 + 1281C^4\beta^9\cos 3\gamma + 3199C^5\beta^{10} \\
& + \frac{1}{3}\big(104C^3\beta^8\cos^2 3\gamma - 308C^4\beta^9\cos^3 3\gamma - 2714C^5\beta^{10}\cos^2 3\gamma\big)\bigg) \\
& + \mathcal{O}\big(\beta^{11}\big), \qquad \text{(A.4)}
\end{aligned}
$$

$$
\begin{aligned}
Q^6\cos^2 3\delta = {} & \left(\frac{3}{4\pi}ZR^2\right)^6\big(\beta^6\cos^2 3\gamma + 6C\beta^7\cos 3\gamma + 6C^2\beta^8\cos^2 3\gamma \\
& + 9C^2\beta^8 + 4C^3\beta^9\cos^3 3\gamma + 16C^3\beta^9\cos 3\gamma \\
& + 21C^4\beta^{10}\cos^2 3\gamma - 6C^4\beta^{10} + 12C^5\beta^{11}\cos^3 3\gamma - 6C^5\beta^{11}\cos 3\gamma \\
& + 4C^6\beta^{12}\cos^4 3\gamma - 4C^6\beta^{12}\cos^2 3\gamma + C^6\beta^{12}\big) \\
\approx {} & q_0^6\big(\beta^6\cos^2 3\gamma + 6C\beta^7\cos 3\gamma + 54C^2\beta^8\cos^2 3\gamma + 9C^2\beta^8 \\
& - 60C^3\beta^9\cos^3 3\gamma + 304C^3\beta^9\cos 3\gamma + 1365C^4\beta^{10}\cos^2 3\gamma + 426C^4\beta^{10} \\
& - 4020C^5\beta^{11}\cos^3 3\gamma + 8826C^5\beta^{11}\cos 3\gamma + 2308C^6\beta^{12}\cos^4 3\gamma \\
& + 20140C^6\beta^{12}\cos^2 3\gamma + 12673C^6\beta^{12}\big) + \mathcal{O}\big(\beta^{13}\big). \qquad \text{(A.5)}
\end{aligned}
$$

References

[1] D. Cline, Annu. Rev. Nucl. Part. Sci. 36 (1986) 683.
[2] J. Stachel, N. Kaffrell, E. Grosse, H. Emling, H. Folger, R. Kulessa, D. Schwalm, Nucl. Phys. A 383 (1982) 429.
[3] J. Stachel, P. Hill, N. Kaffrell, H. Emling, H. Grein, E. Grosse, C. Michel, H. Wollersheim, D. Schwalm, S. Brüssermann, F. May, Nucl. Phys. A 419 (1984) 589.
[4] T. Czosnyka, D. Cline, C. Wu, Bull. Amer. Phys. Soc. 28 (1983) 745.
[5] K. Kumar, Phys. Rev. Lett. 28 (1972) 249.
[6] D. Cline, C. Flaum, in: K. Shoda, H. Ui (Eds.), Proc. of the Int. Conf. in Nuclear Structure using Electron Scattering and Photoreactions, Sendai, Tohoku University, 1972, pp. 61–82.
[7] P. Regan, C. Beausang, N. Zamtir, R. Casten, Z.J.-Y.A. Yamamoto, M. Caprio, S. Gurdal, A. Hecht, C. Hutter, R. Knechen, S. Langdown, D. Meyer, J. Resler, Phys. Rev. Lett. 90 (2003) 152–502.
[8] F. Pan, J. Drayer, N. Phys. A 636 (1998) 156.
[9] J. Stachel, P. van Isacker, K. Heyde, Phys. Rev. C 25 (1982) 680.
[10] J. Dobaczewski, S. Rohoziński, J. Srebrny, Nucl. Phys. A 462 (1987) 72.
[11] K. Zając, L. Próchniak, K. Pomorski, S. Rohoziński, J. Srebrny, Nucl. Phys. A 653 (1999) 71.
[12] P. Lesser, D. Cline, P. Goodle, R. Horoshko, Nucl. Phys. A 180 (1972) 597.
[13] M. Guidry, P. Butler, R. Donangelo, E. Grosse, Y. El Masri, I. Lee, F. Stephens, R. Diamond, L. Riedinger, C. Bingham, A. Kahler, J. Vrba, E. Robinson, N. Johnson, Phys. Rev. Lett. 40 (1978) 1016.
[14] J. Blanchot, Nucl. Data Sheets 64 (1991) 1.
[15] I. Deloncle, A. Bauchet, M.-G. Porquet, M. Girod, S. Peru, J.-P. Delaroche, A. Wilson, B.J.P. Gall, F. Hoellinger, N. Schulz, E. Gueorguieva, A. Minkova, T. Kutsarova, Ts. Venkova, J. Duprat, H. Sergolle, C. Gautherin, R. Lucas, A. Astier, N. Buforn, M. Meyer, S. Perries, N. Redon, Eur. Phys. J. A 8 (2000) 177.
[16] R. Brenn, H. Spehl, A. Weckherlin, H. Doubt, G. van Middelkoop, Z. Phys. A 281 (1977) 219.
[17] A.E. Kavka, Doctoral thesis, Faculty of Science, Uppsala University, 1989.

[18] C. Wu, D. Cline, T. Czosnyka, A. Bäcklin, C. Baktash, R. Diamond, G. Dracoulis, L. Hasselgren, H. Kluge, B. Kotliński, J. Leigh, J. Newton, W. Phillips, S. Sie, J. Srebrny, F. Stephens, Nucl. Phys. A 607 (1996) 178.
[19] K. Adler, A. Winther, Electromagnetic Excitation, North-Holland, 1975.
[20] C. Fahlander, L. Hasselgren, G. Posnert, J. Thun, Phys. Scr. 18 (1978) 47.
[21] F. McGowan, R. Robinson, P. Stelson, W. Milner, Nucl. Phys. A 113 (1968) 592.
[22] S. Rohoziński, J. Dobaczewski, B. Nerlo-Pomorska, K. Pomorski, J. Srebrny, Nucl. Phys. A 292 (1977) 66.
[23] M. Baranger, K. Kumar, Nucl. Phys. A 122 (1962) 241.
[24] A. Davydov, G. Filippov, Nucl. Phys. 8 (1958) 237.
[25] T. Kaniowska, A. Sobiczewski, K. Pomorski, S. Rohoziński, Nucl. Phys. A 274 (1976) 151.
[26] L. Wilets, M. Jean, Phys. Rev. 102 (1956) 788.
[27] S. Rohoziński, J. Srebrny, K. Horbaczewska, Z. Phys. 268 (1974) 401.